Available online at www.sciencedirect.com
SCIENCE DIRECT®
Biochimica et Biophysica Acta 1615 (2003) 33–59
BIOCHIMICA ET BIOPHYSICA ACTA
BBA
www.bba-direct.com

Review

Lipid membranes with grafted polymers: physicochemical aspects

Derek Marsh[a,*], Rosa Bartucci[b], Luigi Sportelli[b]

[a] Max-Planck-Institut für Biophysikalische Chemie, Abteilung Spektroskopie, Am Fassberg 11, D-37077 Göttingen, Germany
[b] Dipartimento di Fisica and Unità INFM, Università della Calabria, I-87036 Arcavacata di Rende (CS), Italy

Received 7 February 2003; received in revised form 15 May 2003; accepted 26 June 2003

Abstract

Membranes grafted with water-soluble polymers resist protein adsorption and adhesion to cellular surfaces. Liposomes with surface-grafted polymers therefore find applications in drug delivery. The physicochemical properties of polymer-grafted lipid membranes are reviewed with mean-field and scaling theories from polymer physics. Topics covered are: mushroom–brush transitions, membrane expansion and elasticity, bilayer-micelle transitions, membrane–membrane interactions and protein–membrane interactions.

Keywords: Lateral pressure; Elastic constant; Bilayer–bilayer interaction; Protein adsorption; Steric stabilisation; Polyethyleneglycol

1. Introduction

Poly(ethyleneglycol) (PEG) is an inert, water-soluble polymer that finds extensive application as a biocompatible coating. Surface-grafted PEG-polymers resist protein adsorption and adhesion to cellular surfaces. Phosphatidylethanolamine *N*-derivatised in the headgroup with PEG provides a controlled means of varying the polymer grafting density of lipid membrane surfaces simply by changing the mole fraction, X_p, of polymer lipid. Liposomes containing such PEG-lipids resist adsorption of various components of the immune system as well as the interaction with lipoproteins and lipolytic enzymes. This results in a prolonged lifetime in the bloodstream that makes these sterically stabilised liposomes suitable vehicles for drug delivery.

Here we review the physicochemical aspects of liposomes grafted with hydrophilic polymer lipids. How the material properties of the lipid membrane are modified by the presence of polymer lipids is a significant feature in the design of sterically stabilised liposomes. The basic design parameters are the polymer size, n_p, and the grafting density (X_p/A_l), where A_l is the area per lipid molecule. These two parameters govern the transition from the mushroom to brush regimes of polymer surface coverage (see Fig. 1). In the mushroom regime, the polymers consist of non-interacting random coils of Flory radius, R_{F3}, at the membrane surface. In the brush regime, the polymer chains are more densely packed, mutually interact, and extend out from the membrane surface forming a layer of thickness, L.

Both the steric repulsive forces of the grafted surface and the degree of protein adsorption differ greatly between the mushroom and brush regimes. Polymer grafting densities in the brush regime favour steric stabilisation of the liposome. At higher polymer grafting densities, lipid polymorphism comes into play. The bulky hydrophilic headgroups favour formation of micelles by polymer lipids. This leads to a destabilisation of lipid membranes at higher grafting densities.

Many of the ways in which grafted polymers modify the colloidal stability and material properties of lipid membranes can be described by relatively straightforward theories of polymer physics that originate from Flory and De Gennes. This review concentrates on these aspects.

2. Statistical physics of grafted polymers

Theories from polymer physics, starting with those of Flory [1] for free polymers and going on to those of De Gennes [2], Alexander [3] and others for grafted polymers, can be used to characterise the statistical configurations and thermodynamics of the polymer chains. Following the original treatment of polymers grafted on solid surfaces [3,4], two concentration regions of polymer lipid content

* Corresponding author. Tel.: +49-551-201-1285; fax: +49-551-201-1501.
E-mail address: dmarsh@gwdg.de (D. Marsh).

0005-2736/$ - see front matter © 2003 Elsevier B.V. All rights reserved.
doi:10.1016/S0005-2736(03)00197-4

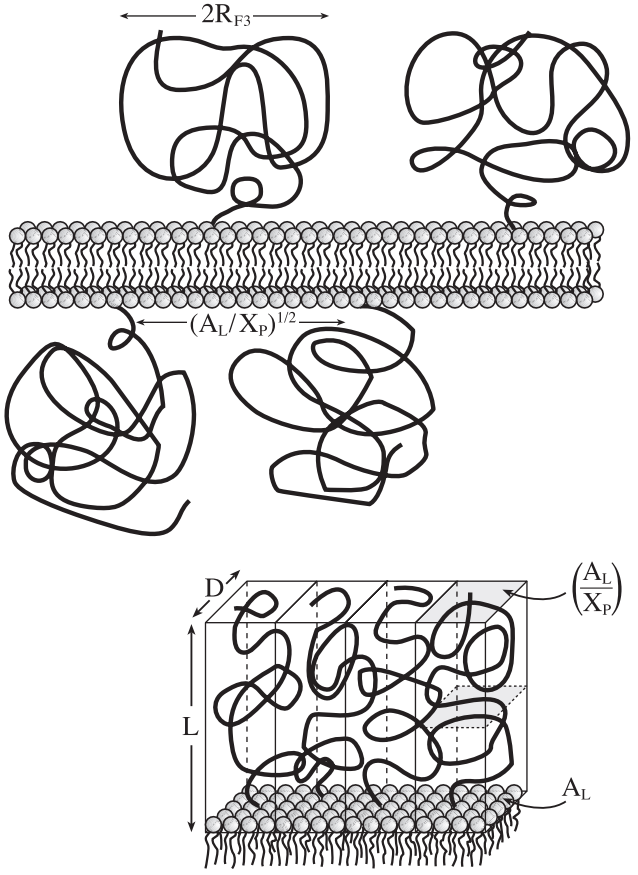

Fig. 1. The mushroom (i.e. low concentration) and brush (i.e. high concentration) regimes of polymer surface grafting. Upper panel: the mushroom regime of non-interacting polymers with radius $\sim R_{F3}$. Lower panel: the brush regime of extended polymer chains of length L, with distance D between grafting points.

may be defined. These are characterised by the so-called "mushroom" and "brush" configurations of the grafted polymer chain (see Fig. 1). The mushroom regime holds at low concentrations of grafted polymer and the brush regime pertains to higher concentrations. The chain configuration in these two regimes may be treated by the methods of polymer physics, as outlined below.

2.1. Mushroom regime

At low concentrations, the polymer headgroups of the grafted lipids do not interact; the polymer has a mushroom-like configuration at the membrane surface. Under these conditions, the polymer chain assumes a random configuration, like that of the polymer free in solution (see Fig. 1, upper panel). The characteristic dimensions of this random coil polymer are specified by the Flory radius, R_F, that is determined by the degree of polymerisation, n_p, and the size, a_m, of the monomer unit [1].

The dimensions of the free polymer are determined by steric interactions (i.e. excluded volume effects) that tend to expand the polymer. These are balanced by the unfavourable entropic effects of stretching the coiled polymer chain. In the Flory theory, the free energy of a real chain is given by (see, e.g. Ref. [2]):

$$F_p/k_BT \approx \frac{v_m n_p^2}{R^3} + \frac{R^2}{n_p a_m^2} \quad (1)$$

where R is the end-to-end distance of the chain and v_m is the excluded volume per monomer. In general, $v_m = a_m^3(1-2\chi)$, where χ is the Flory–Huggins interaction parameter. With an athermal solvent, for which intramolecular interactions other than steric may be neglected $v_m \approx a_m^3$. The first term in Eq. (1) thus represents the excluded volume interactions. These are depicted in a mean-field approximation and are proportional to the square of the local monomer concentration [2]. The second term in Eq. (1) represents the stretching free energy. It is derived from the entropy of an ideal polymer chain the ends of which undergo a (Gaussian) random walk (see Ref. [2]).

Minimising the free energy in Eq. (1) with respect to R, yields the following expression for the (three-dimensional) Flory radius:

$$R_{F3} \approx a_m n_p^{3/5} \quad (2)$$

Hristova and Needham [5] find that for the oxyethylene monomer unit of PEG: $a_m \approx 0.35$ nm. From adhesion measurements, Evans et al. [6] find that the data for PEG lipids is best fitted by a value of $a_m = 0.43$ nm. These values are close to the size of an oxyethylene unit $a_m \approx 0.39$ nm determined from the monomer volume in aqueous solution [6]. This intermediate value is adopted in what follows. Note, however, that a_m effectively scales the relative contributions of the excluded volume and stretching terms in Eq. (1). The Flory radius for PEGs of molecular weight 350, 750, 2000 and 5000 is $R_{F3} = 1.4$, 2.1, 3.8, and 6.7 nm, respectively (i.e. for $n_p = 8$, 17, 45 and 114, with $a_m = 0.39$ nm). For comparison, the heights of the polymer layer measured in the interdigitated mushroom regime of PEG:350, PEG:750 and PEG:2000 distearoyl phosphatidylethanolamine (DSPE) lipids are given in Table 1 [7,8].

Table 1
Thickness, $d_f/2$, of the polymer layer obtained by X-ray diffraction for DSPE-PEG:n_{PEG} lipids in DSPC bilayer membranes [7]

n_{PEG}	X_{PEG}	regime	$d_f/2$ (nm)[a]	R_{F3} (nm)[b]	L (nm)[c]
8	0.1	mushroom[d]	2.0	1.4	(1.0)
17	0.015	mushroom[d]	2.45	2.1	(1.1)
45	0.005	mushroom[d]	3.75	3.8	(2.1)
45	0.1	brush	6.6	(3.8)	5.6
114	0.05	brush	8.8	(6.7)	11.2

R_{F3} is the Flory radius of the polymer and L is the height of the polymer brush.

[a] Half the fluid-layer thickness at the lowest applied osmotic pressures giving contact.

[b] From Eq. (2) with $a_m = 0.39$ nm.

[c] From Eqs. (6) or (10) with $a_m = 0.39$ nm and $A_l = 0.48$ nm^2 (gel phase).

[d] Interdigitated mushrooms.

Eq. (2) applies to the polymer chain free in three dimensions. Confining the polymer chain to one or two dimensions reduces the exponent of R in the first term of Eq. (1) to the appropriate dimensionality. In general, the exponent of n_p in Eq. (2) for $R_{F\hat{d}}$ is given by [2]:

$$\nu = 3/(\hat{d}+2) \tag{3}$$

where $\hat{d}$ is the dimensionality. For three, two and one dimensions: $\nu = 3/5$, 3/4 and 1, respectively. The one-dimensional case will be relevant later for discussion of the brush regime, and the two-dimensional case applies to compressed mushrooms.

2.2. Transition from mushroom to brush regime

When the concentration of the grafted lipid is increased, the polymer headgroups begin to interact and assume a more stretched (i.e. brush) configuration in which the polymer chains extend out from the membrane surface (see Fig. 1, lower panel). The transition between the mushroom and brush regimes occurs at the concentration of grafted lipid for which the surface-associated polymer chains first begin to overlap. This condition is fulfilled approximately at mole fractions, $X_p^{m\rightarrow b}$, of polymer lipid given by:

$$X_p^{m\rightarrow b} > (A_l/\pi a_m^2) n_p^{-6/5} \tag{4}$$

where A_l is the membrane surface area per lipid molecule. The latter is given by $A_l \sim 0.6-0.7$ nm^2 for lipids in the fluid phase and $A_l \sim 0.40-0.48$ nm^2 for lipids in the gel phase [9]. For PEG lipids with polymer molecular weights 350, 750, 2000 and 5000 (i.e. $n_p = 8$, 17, 45 and 114), the transition from mushroom to brush configurations is expected to be initiated at $X_{PEG}^{m\rightarrow b} = 0.11$, 0.045, 0.014 and 0.005, respectively, assuming fluid-phase membranes.

Fig. 2 shows the predictions of Eq. (4) for the transition between mushroom and brush regimes of polymer grafting density (see also Ref. [7]). The mole fraction of polymer lipid, $X_p^{m\rightarrow b}$, at which the brush is first formed decreases strongly with increasing size, n_p, of the grafted polymer. The transition region within the mushroom regime at which polymers from opposing bilayer surfaces are no longer able to interdigitate is indicated by the dashed line in Fig. 2. This occurs at mole fractions of polymer lipid that are half those for the mushroom to brush transition. Only for rather short PEG-lipids (e.g. PEG:350), or at low mole fractions, is the mushroom configuration likely to be of overwhelming significance.

The mushroom regime is revealed as a short region of constant lipid chain mobility in gel-phase dipalmitoyl phosphatidylcholine membranes on admixture with small amounts of PEG:350-dipalmitoyl phosphatidylethanolamine (see Fig. 6, given later). A sharp increase in chain mobility is found from spin-label EPR spectroscopy at ca. 7 mol% of PEG-lipid that corresponds to a decrease in the lipid chain packing density in the brush regime [10]. This correlates

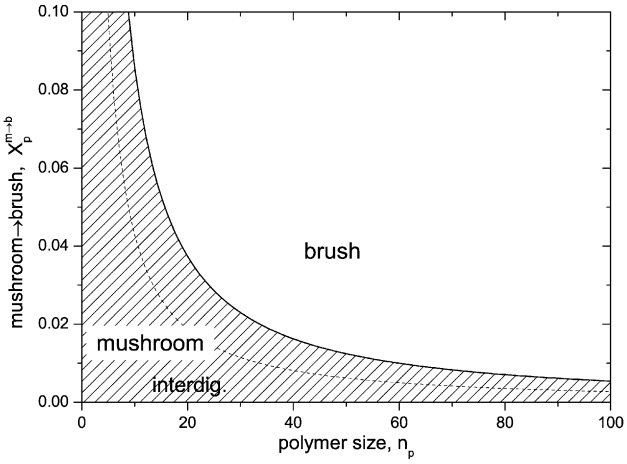

Fig. 2. Mushroom and brush regimes of polymer grafting density as a function of polymer size, n_p, predicted from Eq. (4) with $A_l = 0.65$ nm^2 and $a_m = 0.39$ nm (solid line). The y-axis is the mole fraction, X_p, of polymer lipid in fluid-phase membranes. The dashed line is the border between non-interdigitated mushrooms and those from opposing bilayer surfaces that are fully interdigitated.

reasonably well with a transition from the mushroom to brush regime at $X_{PEG}^{m\rightarrow b} = 0.08$, that is predicted from Eq. (4) for gel-phase phosphatidylcholine lipids and $n_p = 8$ (i.e. PEG:350). The position of the discontinuity moves to lower mole fractions of PEG-lipid with increasing polymer chain length in agreement with Eq. (4) [10], although this transition then begins to overlap with the bilayer to micelle transition. Recent measurements at closer concentration intervals have revealed that the midpoint of the mushroom to brush transition scales according to the polymer length, n_p, with an exponent of ca. -0.8 [11]. This is less steep than the exponent of $-6/5$ predicted from Eq. (4), but of a similar magnitude.

2.3. Mean-field theory for the brush regime

Two different treatments have been given for the polymer chain packing density in the brush regime. The first is a mean field theory that in essence is similar to that presented in Eq. (1). The second is a scaling theory that was given by Alexander and De Gennes et al. [2–4]. The mean-field theory is presented in this section and scaling theory in the following section.

In the brush regime, the polymer chains are extended and the problem is essentially one-dimensional. The chains are confined in the direction normal to the surface of grafting (see the lower panel of Fig. 1). For a grafted polymer chain, the one-dimensional version of the mean-field expression for the free energy is (cf. Eq. (1) and Ref. [12]):

$$F_p^{MF}(R)/k_BT \approx \nu_m \left(\frac{X_p}{A_l}\right)\frac{n_p^2}{R} + \frac{R^2}{n_p a_m^2} \tag{5}$$

where X_p is the mole fraction of polymer lipid and A_l is the area per lipid molecule at the grafting surface. Minimising

the free energy of Eq. (3) with respect to R yields the following expression for the equilibrium length of the polymer chain:

$$L^{\mathrm{MF}} \approx n_{\mathrm{p}} a_{\mathrm{m}}^{5/3} (X_{\mathrm{p}}/A_{\mathrm{l}})^{1/3} \tag{6}$$

when $v_{\mathrm{m}} \approx a_{\mathrm{m}}^3$, appropriate to an athermal solvent (i.e. for $\chi = 0$). The length of the polymer chain is therefore linear in n_{p}, consistent with Eq. (3) for the one-dimensional situation. In Eq. (6), it is tacitly assumed that the monomer density is uniform throughout the brush. Hence, L^{MF} is equivalent to the length of the brush region. The corresponding equilibrium free energy per polymer is given from Eqs. (5) and (6), with $R = L^{\mathrm{MF}}$:

$$F_{\mathrm{p}}^{\mathrm{MF}}(L)/k_{\mathrm{B}}T \approx n_{\mathrm{p}} a_{\mathrm{m}}^{4/3} (X_{\mathrm{p}}/A_{\mathrm{l}})^{2/3} \tag{7}$$

As will be seen later, the dependence of the mean-field free energy on A_{l} (and on X_{p}) differs from that for the scaling theory.

Milner et al. [12,13] have developed a self-consistent mean-field (SCMF) theory for dense polymer brushes. In this treatment, the distribution of polymer chain end positions is considered explicitly. They find that the density distribution of chain segments is parabolic with vertical position, z, in the brush:

$$\Phi(z) = [\pi^2/8 n_{\mathrm{p}}^2 a_{\mathrm{m}}^3]\left[(L^{\mathrm{MF}})^2 - z^2\right] \tag{8}$$

This contrasts with the assumption of a step-function profile that was made tacitly above, as is illustrated in Fig. 3 (see also Ref. [14]). In Eq. (8), the value of L^{MF} is identical to that given above in Eq. (6), where the constant premultiplying factor is explicitly $(12/\pi^2)^{1/3} = 1.07$. Now, however, L^{MF} multiplied by this factor is the *maximum* extension of the polymer chains, i.e. the maximum thickness of the brush region. An expression identical to Eq. (7) is obtained for the free energy in the self-consistent field treatment. The constant premultiplying factor in Eq. (7) is then explicitly $(9/10)(\pi^2/12)^{1/3} = 0.84$. A word of caution is perhaps necessary, however, with respect to the explicit multiplicative factors. As already mentioned, parameterisation in terms of a_{m} implicitly includes a scaling of the strengths of the excluded volume and chain stretching contributions to the mean field (or scaling theory) free energy (cf. Ref. [3]). A more general formulation of Eq. (5) is given later in connection with bilayer–bilayer interactions. There, a multiplicative factor scaling the relative strengths of the steric exclusion and stretching terms is included explicitly (see Section 6.3.1).

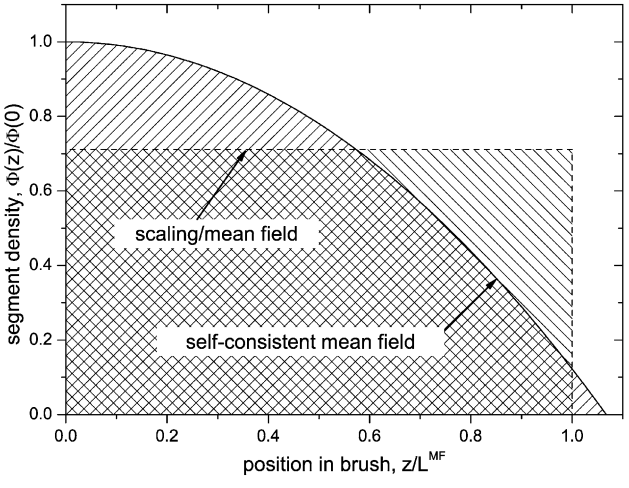

Fig. 3. Distribution of the polymer segment density in the polymer brush. The vertical height from the membrane surface is z. Solid line: the profile given by Eq. (8) from the SCMF theory of Milner et al. [13]. Dashed line: profile assumed in the simple mean-field and scaling theories. The position axis is scaled by L^{MF} that is given by Eq. (6).

2.4. Scaling theory for the brush regime

The essential determinant in the scaling theory is the one-dimensional nature of the problem for the polymer chains confined in the brush regime (see Fig. 1, lower panel). Under these conditions, the length, L, of the polymer chains and the free energy of the chains is linear in the degree of polymerisation, n_{p}. This result for L follows immediately from Eq. (3) for one-dimensional confinement. That for the free energy follows, e.g. from considering the stretched chain as a one-dimensional array of blobs of which the corresponding sections of the chain are coiled in a manner similar to that for a three-dimensional chain [2].

For long polymer chains, the scaling law for the equilibrium length is given by [2,15]:

$$L^{\mathrm{SC}} \approx R_{\mathrm{F3}} (R_{\mathrm{F3}}/D)^{m_{\mathrm{L}}} \tag{9}$$

where D is the diameter of the confinement, i.e. the distance between polymer grafting points. The length scale in the problem is the Flory radius, R_{F3}, given by Eq. (2). From this and the requirement that L^{SC} must be linear in n_{p}, the exponent in the scaling law is given by $m_{\mathrm{L}} = 2/3$. In terms of mole fraction of polymer lipid, the distance D between grafting points is given by $D^2 = A_{\mathrm{l}}/X_{\mathrm{p}}$ (see Fig. 1, lower panel). Eq. (9) then becomes:

$$L^{\mathrm{SC}} \approx n_{\mathrm{p}} a_{\mathrm{m}}^{5/3} (X_{\mathrm{p}}/A_{\mathrm{l}})^{1/3} \tag{10}$$

This is exactly the same result as obtained from mean field theory that is given in Eq. (6). Table 1 compares the predictions of the height of the polymer brush from Eqs. (6) or (10) with measurements by X-ray diffraction [7] for multibilayers containing DSPE-PEG:2000 and DSPE-PEG:5000. The X-ray measurements were made at applied osmotic pressures for which the polymer brushes from opposing lipid surfaces first come into contact.

The corresponding scaling law for the free energy for long polymer chains is given by [2,15]:

$$F_{\mathrm{p}}^{\mathrm{SC}} \approx k_{\mathrm{B}}T (R_{\mathrm{F3}}/D)^{2m_{\mathrm{F}}} \tag{11}$$

where (also above) k_B is Boltzmann's constant and T is the absolute temperature. From Eq. (2) and the requirement that the free energy is linear in n_p, one obtains $2m_F = 5/3$ (the factor 2 multiplying m_F is arbitrary. It is used simply for convenience and consistency with what follows). In terms of mole fraction of polymer lipid and area per lipid molecule, the free energy per polymer is therefore given by:

$$F_p^{SC}/k_BT \approx n_p a_m^{5/3}(X_p/A_l)^{5/6} \quad (12)$$

This scaling-law result differs from that obtained from mean-field theory, i.e. Eq. (7). The difference arises from the inclusion of correlations between segments (in the "blobs") in the scaling theory. Both expressions, however, are linear in n_p. A further difference between the scaling theory and the SCMF treatment of Milner et al. [12,13] is in the distribution of chain ends. In the former case—apart from an initial depletion layer—the distribution is essentially a constant step function [4], whereas in the latter case, the distribution has a parabolic form given by Eq. (8).

In principle, Eq. (12) applies to the excluded volume effect of confinement because the characteristic length in the treatment is R_{F3}. Alexander [3] has derived a scaling law for the stretching contribution to the chain free energy. At equilibrium, this has the same scaling dependence as the excluded volume term, as it must. Both terms are considered separately later in connection with membrane–membrane interactions (Section 6.3.2).

Hansen et al. [16] have proposed practical criteria for the applicability of scaling theory that are derived from osmotic pressure data on the free polymer in aqueous solution. According to scaling theory, the osmotic pressure depends on volume fraction of free polymer as $\Pi_f \sim \phi_f^{9/4}$ [2]. This semi-dilute power law holds for a very long polyoxyethylene polymer, PEG:20,000, over a wide range of ϕ_f. For shorter PEG-polymers, the scaling law holds only at progressively higher values of ϕ_f as the polymer length decreases. In a polymer brush, the volume fraction of monomers given from Eq. (10) by scaling theory is: $\bar{\phi}_p \approx a_m^{4/3}(X_p/A_l)^{2/3}$. From this and the osmotic pressure results, the scaling regime for grafted polymer requires that the mole fraction of polymer lipid is $X_p \geq 0.23$ and 0.07–0.10 for DSPE-PEG:2000 and DSPE-PEG:5000, respectively [16]. These values are upper estimates because it is likely that the independence of monomer volume fraction from polymer length is achieved more readily in the brush regime for a surface-tethered polymer than for a polymer free in solution in three dimensions.

3. Membrane expansion by the polymer brush

Steric interactions between the grafted polymers in the brush regime will give rise to a lateral pressure, Π_p, which will tend to expand the lipid membrane. Amongst other things, this will change the permeability properties and shift the chain-melting transition of the membrane. Experimental evidence for such a lateral expansion is provided by the increase in motional freedom of spin-labelled lipid chains on incorporating polymer-grafted lipids in bilayer membranes [10]. In phospholipid monolayers, the increase in lateral pressure by PEG-lipids at constant surface density has been measured directly using surface balance techniques [17]. The magnitude of the lateral pressure is given by the first derivative of the free energy of the polymer brush (Eqs. (7) and (12)) with respect to the membrane area. For long polymers and/or high polymer-lipid contents this can reach appreciable values, relative to the equivalence pressure ($\sim$ 35 mN m^{-1}; Ref. [18]) between lipid monolayers and bilayers [19]. The extent of the resulting membrane expansion is determined by the lipid equation of state, i.e. by the monolayer Π–A isotherm at the bilayer equivalence pressure. Here we follow previous work [10] by using a simple model equation of state due to Israelachvili et al. [20], in order to illustrate the basic principles. A more precise treatment using a virial equation of state is given by Marsh [19].

3.1. Equilibrium surface area

The increase in surface area of the lipid membrane that is induced by grafting polymer chains is estimated by using a simple model introduced by Israelachvili et al. (see Ref. [20]). This model adequately describes the elastic properties of fluid membranes in the absence of headgroup-grafted polymers (see Refs. [18,21] for a discussion). The interfacial free energy per lipid molecule in the membrane is given by:

$$F_{int}^{tot}/k_BT = (\gamma/k_BT)A_l + C_o/A_l + X_p.F_p^{brush}/k_BT \quad (13)$$

where the first two terms represent the interfacial free energy of the polymer-free membrane. The first term is the cohesive free energy of the membrane. Here, γ is the hydrophobic free energy density which has a value $\gamma \sim 3.9 \times 10^{-20}$ J nm^{-2} [18]. The second term represents the net repulsive interactions between non-polymer lipid molecules. This is represented by an inverse dependence on the area, A_l, per lipid molecule. The equilibrium area per lipid molecule, $A_{l,o}$, in the absence of the polymer brush is given by (see Ref. [21]):

$$A_{l,o} = \sqrt{C_o k_B T/\gamma} \quad (14)$$

This has values in the region of $A_{l,o} \sim 0.6$–0.7 nm^2 for fluid lamellar phospholipid membranes [9]. The final term in Eq. (13) is the free energy per lipid molecule of the polymer brush, where X_p is the mole fraction of polymer lipids. This term is given from Eqs. (7) and (12) as:

$$X_p.F_p/k_BT = a_m^{2m_F} n_p X_p^{m_F+1}/A_l^{m_F} \quad (15)$$

where $m_F = 5/6$ for the scaling theory (i.e. Eq. (12)) and $m_F = 2/3$ for mean-field theory (i.e. Eq. (7)).

The equilibrium area per lipid molecule in the presence of the polymer brush is given by minimising the total interfacial free energy, F_{int}^{tot}, with respect to A_l. This yields the following result:

$$A_l^2 = A_{l,o}^2 + m_F \frac{k_B T}{\gamma} a_m^{2m_F} n_p X_p^{m_F+1} A_l^{1-m_F} \quad (16)$$

where the second term on the right represents the increase in area per lipid induced by the polymer brush. The area per lipid molecule increases monotonically with increasing mole fraction of polymer lipid, with a steadily increasing gradient (see Fig. 4, below). To first order, the expansion ($\Delta A_l = A_l - A_{l,o}$) in area per lipid molecule by the polymer brush is given by:

$$\frac{\Delta A_l}{A_{l,o}} \approx m_F \frac{k_B T}{K_A^o} a_m^{2m_F} n_p \left(\frac{X_p}{A_{l,o}}\right)^{m_F+1} \quad (17)$$

which is directly proportional to the degree of polymerisation, n_p, and scales with the $(m_F + 1)$th power of the mole fraction of polymer lipid. Here K_A^o $(= 2\gamma)$ is the area expansion elastic modulus of a single lipid layer (see next section). To first order, this expression holds good for a general value of K_A^o (i.e. for a general exponent of A_l in the C_o term of Eq. (13)). Eq. (17) agrees with the leading term obtained by Hristova and Needham [5] for mean-field theory. The treatment of the latter authors differs from Eq. (16) in higher order because they assumed a fixed area expansion modulus, K_A. In the present treatment, K_A is allowed to vary according to the explicit dependence of the free energy on A_l that is given by Eq. (13). It should be noted that the assumption of constant K_A has been demonstrated experimentally only up to values of $\Delta A_l/A_{l,o} \sim 0.05$, which is the maximum extension that giant lipid vesicles can support in pipette aspiration experiments (see, e.g. Ref. [22]). Over this range, both treatments yield very similar results for the area expansion.

The area expansion is given as a function of polymer grafting density, X_p in Fig. 4. Results from Eq. (16) for the scaling theory and mean-field theory are compared in this figure. The calculations retain all quadratic terms in $\Delta A_l/A_{l,o}$ and are correct to second order in the area expansion. The range of validity of the first-order approximation given by Eq. (17) is also indicated in the figure. Note that the x-axis differs somewhat between the scaling and mean-field theories because of the factor $n_p^{1/(m_F+1)}$. The range of polymer lipid contents shown in Fig. 4 encompasses those for which micelles are formed (see later). An area increase of 5% is achieved at mole fractions of $X_p \approx 0.49$ (0.46), 0.19 (0.16) and 0.12 (0.09) for polymer lengths of $n_p = 8$, 45, 114,

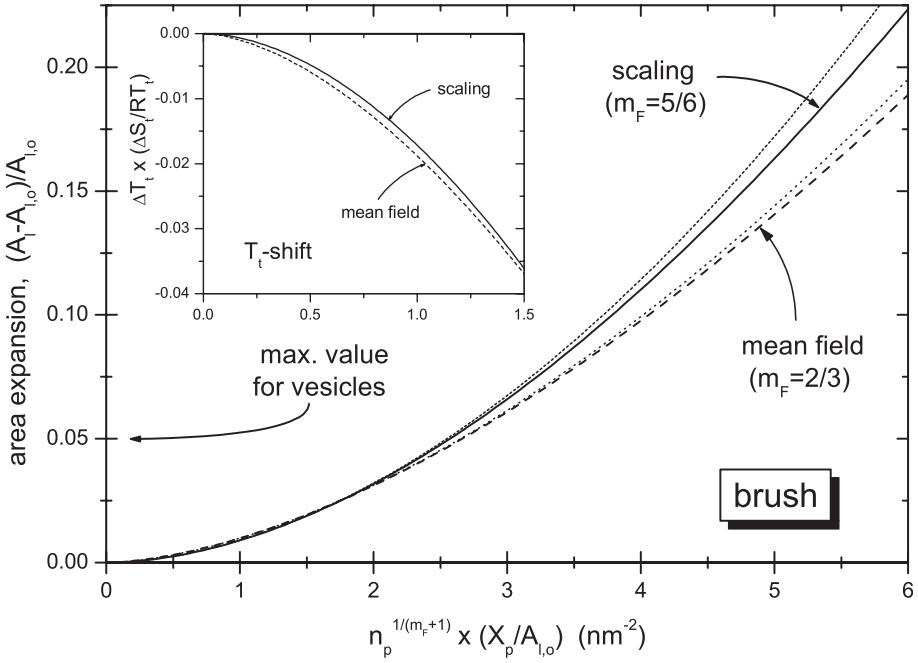

Fig. 4. Dependence of the fractional increase, $(A_l - A_{l,o})/A_{l,o}$, in area per lipid molecule by the lateral pressure in the polymer brush, as a function of the mole fraction, X_p, of polymer lipid. Calculations are made using Eq. (16) with $a_m = 0.39$ nm, $\gamma = 3.9 \times 10^{-20}$ J nm^{-2} ($K_A^o = 78$ mN.m^{-1}) and $T = 293$ K, and are correct to second order in the area extension. Solid line is the prediction from scaling theory and the dashed line that from mean-field theory. The first-order approximation (i.e. Eq. (17)) is given by the short-dashed line (scaling theory) and the dotted line (mean-field theory). Full-scale of the x-axis corresponds to $X_p = 1.16$ (1.03), 0.45 (0.37) and 0.27 (0.21) for polymer sizes $n_p = 8$, 45 and 114 in the scaling (mean-field) theory, with $A_{l,o} = 0.6$ nm^2. Insert: shift (ΔT_t) in chain-melting transition temperature of bilayer membranes predicted from Eq. (19). Full scale of the x-axis (i.e. $n_p^{1/(m_F+1)} X_p/A_l$) corresponds to $X_p = 0.27$ (0.24), 0.10 (0.09) and 0.06 (0.05) for polymer sizes $n_p = 8$, 45 and 114 in the scaling (mean field) theory, with $A_l = 0.55$ nm^2. For dipalmitoyl phosphatidylcholine membranes, the factor scaling the y-axis is: $\Delta S_t/RT_t = 0.044$ K^{-1}.

respectively, as predicted by scaling (mean-field) theory. This maximum area extension supported by giant lipid vesicles was used by Hristova and Needham [5,23] as a criterion to define the saturation concentration of polymer lipid in a lamellar phospholipid membrane. These values are greater than those for the onset of micelle formation in PEG-lipid/phosphatidylcholine mixtures (see later).

3.2. Shift in chain-melting transition

The lateral expansion induced by the polymer brush in gel-phase membranes also causes a lowering of the lipid chain-melting temperature, T_t. A perturbation calculation shows that the shift in transition temperature is related directly to the lateral pressure: $\Pi_p^{brush} = -X_p.\partial F_p^{brush}/\partial A_l$, contributed by the polymer brush (see, e.g. Ref. [21]):

$$\Delta T_t = -N_A(\Pi_p^{brush}/\Delta S_t)\Delta A_t \tag{18}$$

where ΔA_t is the increase in area per lipid molecule on chain melting, N_A is Avogadro's number, and ΔS_t is the transition entropy for chain melting. From Eqs. (15) and (18), the shift in chain-melting transition temperature induced by the polymer lipid is therefore given by:

$$\Delta T_t = -\frac{N_A k_B T_t}{\Delta S_t}\left(\frac{\Delta A_t}{A_l}\right)\left(\frac{a_m^2}{A_l}\right)^{m_F} m_F.n_p X_p^{m_F+1} \tag{19}$$

Typical mean values for the lipid molecular area and its change on chain melting are: $A_l \approx 0.55$ nm^2 and $\Delta A_t/A_l \approx 0.18$, respectively, e.g. for phosphatidylcholines [9]. The insert in Fig. 4 gives the dependence of the shift in transition temperature on polymer size and content that is predicted by Eq. (19). The polymer brush is predicted to lower the chain-melting transition because it exerts a positive lateral pressure in the membrane. For admixture of PEG-lipids with hydrocarbon chains identical to those of the host lipid, this is the direction of the shift that is observed experimentally [10,24].

Longer polymer lipids create a greater lateral pressure and therefore are more effective in reducing the transition temperature. As will be seen later, however, larger amounts of the shorter polymer lipids can be incorporated into the membrane prior to micelle formation. The calculations given in the insert of Fig. 4 approximately cover the range of possible polymer-lipid contents for DPPC mixed with PEG-DPPE lipids of different sizes, whilst preserving a lamellar phase. They also correspond to the range over which a perturbation treatment (i.e. Eq. (18)) is acceptable. Taking calorimetric values of $\Delta S_t = 115$ J mol^{-1} K^{-1} and $T_t = 314$ K, appropriate to dipalmitoyl phosphatidylcholine (see, e.g. Ref. [9]), yields predicted shifts that are relatively modest, on the order of 1–2°, in agreement with experimental measurements for sub-micellar contents of polymer lipid [24,25]. Nevertheless, small shifts in chain-melting temperature are of practical relevance to the design of liposomes for controlled release of contents by mild hyperthermia [26,27].

4. Elastic constants of polymer-grafted membranes

Stretching of the grafted polymers and their mutual interactions in the brush regime will modify the elastic properties of the composite membrane with respect both to area dilation and to bending of the membrane. This direct contribution of the polymer brush to the net membrane elasticity has been treated by Hristova and Needham [23] and by Milner et al. [13]. From the discussion in the previous section, it is clear that the lateral pressure in the polymer brush will also tend to expand the lipid membrane and that this, in turn, will modify the intrinsic elastic properties contributed by the lipid chains. This indirect effect of the grafted polymer can be treated by combining estimates of the lateral pressure from polymer physics with the equation of state for the lipid layer. Such an approach has been given by Marsh [19] by using a virial expansion for the lipid equation of state. Here we use the simpler equation of state introduced by Israelachvili et al. [20]—see Eq. (13)—to illustrate the basic principles.

4.1. Stretching elasticity

The elastic area extension modulus is an important quantity because it characterises the elastic deformations of the membranes in response to lateral tension [28]. In particular, it can affect vesicle permeability and the insertion of amphiphilic molecules and proteins in the membrane [18]. These elastic properties can be modified significantly, relative to normal phospholipid bilayer membranes, by the lateral pressure in the polymer brush. Currently, there is only one measurement of the area elastic modulus in membranes containing polymer lipids [29]. Little relative change was found in the expansion modulus at the level of 4 mol% PEG-lipid. Sizeable changes have been predicted for the direct contribution from the polymer [23], but it will be seen below that this is offset by the lateral expansion that the polymer brush induces in the lipid layer.

The area extension modulus, K_A, is related to the interfacial free energy by (see Refs. [21,28]):

$$K_A = 2A(\partial^2 F_{int}/\partial A^2)_T \tag{20}$$

The factor of two is included to sum the contributions from both monolayers of the bilayer lipid membrane. From Eq. (13), the elastic constant for area dilation is therefore given by:

$$K_A = K_A^o\left(\frac{A_{l,o}}{A_l}\right)^2 + 2m_F(m_F+1)\frac{k_B T}{A_l}\left(\frac{a_m^2}{A_l}\right)^{m_F} n_p X_p^{m_F+1} \tag{21}$$

where K_A^o ($=4\gamma$) is the area expansion modulus of the lipid bilayer membrane with no grafted polymer. It is clear from Eq. (21) that the polymer brush makes two opposing contributions to the area elastic constant, relative to that for the ungrafted bilayer membrane. The first contribution arises from the increase in equilibrium area per lipid molecule (in the tension-free state) that was treated in the preceding section. This poises the membrane at a different point in the Π–A curve that is characterised by a smaller value of K_A (cf. Ref. [18]). The second contribution is the elastic response of the polymer brush that is given by the second term on the right-hand side of Eq. (21).

Substituting the $(A_{l,o}/A_l)^2$ term in Eq. (21) from Eq. (16) yields the following result for the area elastic modulus:

$$K_A = K_A^o - \frac{2m_F(1-m_F)k_BTa_p^{2m_F}(A_l^{1-m_F}/A_{l,o}^2)n_pX_p^{m_F+1}}{1+4m_F(k_BTa_p^{2m_F}/K_A^o)(A_l^{1-m_F}/A_{l,o}^2)n_pX_p^{m_F+1}} \tag{22}$$

Because $m_F<1$ in both scaling and mean-field theories, this predicts that the area elastic modulus is reduced by the polymer brush. To first order in the polymer-induced area extension, the reduction in K_A given by Eq. (22) scales directly with polymer length, n_p, and with grafting density according to $(X_p/A_{l,o})^{m_F+1}$. The maximum fractional decrease in K_A according to Eq. (22) is $1/2\ (1-m_F)=1/12$ or 1/6 for the scaling and mean-field theories, respectively. This is not achieved, however, for physically realistic polymer lipid contents. For the range given in Fig. 4, the total decrease in K_A is 2.7% or 5% for the scaling and mean-field theories, respectively. Experimentally, 4 mol% of a PEG:1900 polymer lipid was found to have little effect on the stretching elasticity of a 2:1 mol/mol stearoyl-oleoyl phosphatidylcholine:cholesterol membrane [29]. This is in agreement with Eq. (22) that predicts decreases of 0.03% or 0.1% from the scaling and mean-field approximations, respectively, for $X_p=0.04$, $n_p=43$ and $K_A^o=343$ mN m^{-1} (appropriate to cholesterol-containing membranes).

If the area expansion modulus, K_A^o, of the lipid remains constant, rather than being allowed to vary according to Eq. (13), then the predicted change in K_A is considerably larger and of opposite sign (cf. Eq. (21)). This was the model assumed in the original calculation of Hristova and Needham [23], which unfortunately contains an error of sign. For a constant lipid expansion modulus, the free energy is given by Eq. (13) but with the first two terms replaced by the lipid elastic free energy, $1/2K_A^o(A_l-A_{l,o})^2/A_{l,o}$. The net area expansion modulus in the presence of the polymer brush is then given to second order by:

$$K_A \approx K_A^o + \frac{2m_F(m_F+2)k_BTa_m^{2m_F}n_p(X_p/A_{l,o})^{m_F+1}}{1+2m_F(m_F+1)(k_BT/K_A^o)a_m^{2m_F}n_p(X_p/A_{l,o})^{m_F+1}} \tag{23}$$

It should be remembered that $A_{l,o}$ is the equilibrium area/lipid molecule in the absence of the polymer brush, which is less than the equilibrium value (i.e. the value of A_l in the tension-free state) in the presence of the polymer brush. To first-order, the ratio of the change in expansion modulus predicted for constant lipid K_A to that for variable lipid K_A is $-(m_F+2)/(1-m_F)$ (cf. Eqs. (22) and (23)). This has values of $-17\times$ and $-8\times$ in the scaling and mean-field cases, respectively. The prediction of Eq. (23) for $X_p=0.04$ still, however, represents an increase of only ~ 2–3 mN m^{-1}.

In general, therefore, the grafted polymer does not greatly affect the elastic constant for area expansion, because of the compensating effect on the intrinsic K_A of the lipids. This differs somewhat from previous predictions [23]. Even for very stiff membranes, the relative change is not great because of the higher intrinsic value of K_A. See also Ref. [19].

4.2. Curvature elasticity

The polymer will influence the bending of the grafted membrane in a manner that is expected to depend strongly on the length, L, of the brush region. This can affect both the morphology and stability of a lamellar liposomal membrane. Experimental information on the influence of polymer lipids on curvature elasticity is currently lacking, although strong effects may be anticipated from the known propensity to form micelles (see later sections). The curvature elasticity of polymer-grafted membranes has been analysed in detail theoretically for large curvatures by Hristova and Needham [23], and for normal curvatures by Milner and Witten [30] with their self-consistent field version of mean-field theory. Here, the bending of lamellar membranes, i.e. small curvatures, is considered.

The mean curvature bending modulus, k_c, is given by the second derivative of the free energy with respect to the mean curvature c (i.e. the inverse local radius of curvature, $1/R^{curv}$) according to Refs. [21,28]:

$$k_c = (\partial^2 F_{int}/\partial c^2)_T \tag{24}$$

Therefore, the polymer brush will contribute additively by an amount k_c^p to the curvature elasticity modulus. For continuum or thin shell models, the curvature modulus depends on the area modulus, K_A, and the membrane thickness, d_t, according to Refs. [28,31]:

$$k_c \sim K_A d_t^2 \tag{25}$$

where the scaling constant depends on the distribution of elastic stress across the membrane. This equation may be used as a first approach to establish the scaling laws for the dependence of the curvature modulus on the polymer-lipid parameters.

For long polymers, the thickness of the lipid layer may be neglected. Thus the effective thickness of the membrane is: $d_t \approx 2L$. From Eq. (25), and the expressions given for K_A and L by Eqs. (23) and (6), respectively, the polymer brush

contribution to the mean curvature elasticity modulus scales according to:

$$k_c^p \sim k_B T a_m^{2m_F+10/3} n_p^3 \left(\frac{X_p}{A_l}\right)^{m_F+5/3} \tag{26}$$

This is in agreement with the scaling results obtained by Hristova and Needham [23] with $m_F = 5/6$ for scaling theory, and by Milner and Witten [30] with $m_F = 2/3$ for mean-field theory. In particular, the bending modulus scales as the cube of the degree of polymerisation, i.e. n_p^3, and with a stronger than quadratic dependence on the content of polymer lipid, i.e. $X_p^{(5/3)+m_F}$.

Just as for the area expansion modulus, the bending modulus, k_c^{lipid}, for the lipid component may be modified from the value of k_c^o for a bare lipid bilayer, as a result of the area expansion by the lateral pressure of the polymer brush. The scaling for K_A is given in Eq. (21). For constant lipid volume, the bilayer thickness scales as $d_t \sim 1/A_l$. Therefore, from Eq. (25), the mean curvature modulus of the lipid is given by:

$$k_c^{lipid} = k_c^o (A_{l,o}/A_l)^4 \tag{27}$$

in the presence of the polymer brush. In principle, for high polymer lipid contents, this can represent a considerable reduction relative to the bare lipid membrane.

In a more general treatment of curvature elasticity, the free energy of bending is given by:

$$F_{el}(c_1, c_2) = \frac{1}{2} k_c (c_1 + c_2 - 2c_o)^2 + \bar{k}_c c_1 c_2 \tag{28}$$

where c_1 and c_2 ($\equiv 1/R_1^{curv}$, $1/R_2^{curv}$) are the principal curvatures at a given point, k_c and $\bar{k}_c$ are the elastic moduli for bending (i.e. mean curvature) and Gaussian curvature (i.e, saddle-splay bending), respectively, and c_o ($\equiv 1/R_o^{curv}$) is the preferred or spontaneous curvature. The mean curvature modulus, k_c, already introduced describes cylindrical bending (i.e. $c_1 = c$, $c_2 = 0$). A spherical elastic deformation (i.e. $c_1 = c_2 = c$) involves additionally the Gaussian curvature modulus. Bending into a saddle surface (i.e. $c_1 = -c_2$) involves only the latter, $\bar{k}_c$.

The bending moduli and the spontaneous curvature are related to the lateral pressure distribution, $\Pi_p'(z)dz$, transverse to the membrane, where z is in the direction of the membrane normal. Here the prime represents the derivative of the lateral pressure with respect to position along the membrane normal. The contributions from the grafted polymer are given by the following integrations over the brush region [30,32]:

$$k_c^p = -\int_o^L z \frac{\partial \Pi_p'(z)}{\partial c}\bigg|_{c=0} dz \tag{29}$$

$$\bar{k}_c^p = -\int_o^L z^2 \Pi_p'(z) dz \tag{30}$$

$$2k_c c_o^p = \int_o^L z \Pi_p'(z) dz \tag{31}$$

Thus, only k_c depends on the properties of the curved membrane, whereas $\bar{k}_c$ and $k_c c_o$ are determined by properties of the unbent membrane alone [30].

4.2.1. Mean curvature modulus

The lateral pressure (which has the opposite sign to the osmotic pressure or lateral stress) may be obtained from the free energy of the polymer brush (i.e. Eq. (15)) according to: $\Pi_p(z) = -X_p(\partial F_p^{brush}(z)/\partial A_l(z))$. The area per lipid molecule at a height z from the lipid surface into the polymer brush is given for cylindrical geometry by:

$$A_l(z) = A_l(1 + zc) \tag{32}$$

where A_l is the area at the lipid surface (strictly speaking, the neutral surface) and $c = 1/R^{curv}$ is the membrane curvature. From Eqs. (15) and (32):

$$\frac{\partial \Pi_p'(z)}{\partial c} = -m_F(m_F+1) k_B T a_m^{2m_F} n_p \left(\frac{X_p}{A_l}\right)^{m_F+1} \tag{33}$$

where $\Pi_p'(z) = \partial \Pi_p / \partial z$. Substituting in Eq. (29) and using Eq. (6) for the length of the polymer brush in the integration limit yields:

$$k_c^p = \frac{m_F(m_F+1)}{2} k_B T a_m^{2m_F+10/3} n_p^3 \left(\frac{X_p}{A_l}\right)^{m_F+5/3} \tag{34}$$

for the polymer contribution to the mean curvature elastic modulus. This is in complete agreement with the straightforward scaling arguments that led to Eq. (26). Eq. (34) applies to a lipid monolayer. For a bilayer membrane, the bending modulus is twice this value. Note that application of Eqs. (29) and (32) to the lipid contribution to the bending modulus, where the free energy is given by the first two terms of Eq. (13), also yields the result already given by Eq. (27). When expressed in a more general way that explicitly includes the dependence on area expansion modulus, viz.: $k_c^L = k_c^o (K_A^L/K_A^o)\ (A_{l,o}/A_l)^2$, it is independent of the form assumed for the lipid equation of state [19].

The polymer-lipid contribution, k_c^p, to the bending modulus predicted by Eq. (34) is given as a function of the polymer grafting density in Fig. 5. For short polymers with $n_p \leq 8$, this contribution never exceeds the bending modulus, k_c^o, of bare lipid membranes. Experimental values for the latter lie in the region $k_c^o \sim 1\text{–}2 \times 10^{-19}$ J [9]. For long polymers, e.g. PEG:2000 or PEG:5000, the polymer-lipid contribution can exceed that of the bare lipid membrane because of the cubic dependence on n_p. The crossover point occurs at polymer-lipid contents of $X_p = 0.11\text{–}0.16$ and $X_p = 0.04\text{–}0.03$ for $n_p = 45$ and 114, respectively. These values, however, are comparable to those at which micelle formation begins in polymer-lipid membranes with phosphatidylcholine (see later). Calculations

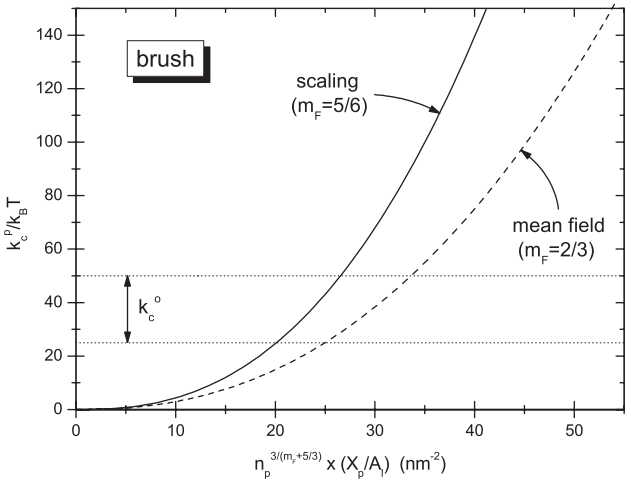

Fig. 5. Dependence of the polymer-lipid contribution, k_c^p, to the mean curvature elastic modulus on the mole fraction, X_p, of polymer lipid. Calculations are made using Eq. (34) multiplied by a factor of two for bilayers, with $a_m = 0.39$ nm and $T = 293$ K. Solid line is the prediction from scaling theory and the dashed line that from mean-field theory. The horizontal dotted lines indicate the approximate experimental range for the bending modulus, $k_c^o \sim 1-2 \times 10^{-19}$ J, of bare lipid bilayers. Full scale of the x-axis corresponds to $X_p = 2.94$ (2.47), 0.37 (0.27) and 0.12 (0.08) for $n_p = 8$, 45, 114 in the scaling (mean-field) theory, with $A_l = 0.65$ nm^2.

using the virial lipid equation of state indicate that for $n_p = 8$ the net value of k_c decreases but only very little with increasing polymer-lipid content [19]. For longer polymer lipids, k_c is increased only slightly at polymer-lipid contents corresponding to the onset of micellisation, but exceeds k_c^o several or many times depending on polymer length for compositions corresponding to the micellar phase.

4.2.2. Gaussian curvature modulus

Of additional interest are the curvature elastic properties $\bar{k}_c$ and c_o, which have not been previously considered. These depend on the constant surface pressure distribution in the polymer brush, $\Pi_p'(z) = \Pi_p(z)/L$. From Eq. (30), it is then found that:

$$\bar{k}_c^p = -2/3 k_c^p/(m_F + 1) \tag{35}$$

Hence, the Gaussian curvature modulus scales with the polymer properties exactly as does the mean curvature modulus. This is a result already obtained by Milner and Witten [30] and Hristova and Needham [23]. Again Eq. (35) applies to a monolayer, and for a bilayer $\bar{k}_c^p$ is twice this value. The sign of $\bar{k}_c$ is such that formation of saddle surfaces (for which $c_1 = -c_2$) costs free energy, just as for simple cylindrical bending (see also Ref. [30]). As for the mean curvature modulus, lateral expansion of the membrane by the polymer brush leads to a reduction in the lipid contribution to $\bar{k}_c$. The reduction factor, however, is different from that for k_c (cf. Eqs. (29) and (30)). It is given by $\Pi_{lipid}/\Pi_{lipid}^o (A_{l,o}/A_l)^2$, where Π_{lipid} and Π_{lipid}^o are the lateral pressures corresponding to A_l and $A_{l,o}$, respectively, which are deduced from the lipid equation of state [19]. Qualitatively, the effects on the total Gaussian curvature modulus are similar to those discussed already for k_c.

4.2.3. Spontaneous curvature

The spontaneous bending moment $2k_c c_o^p$ is obtained from Eq. (31) in exactly the same way as for the Gaussian curvature modulus. The spontaneous curvature induced by the grafted polymer is then given by:

$$c_o = \frac{1}{4} m_F \frac{k_B T}{k_c} a_m^{2m_F+5/3} n_p^2 \left(\frac{X_p}{A_l}\right)^{m_F+4/3} \tag{36}$$

where k_c is the total mean curvature modulus, including the contribution from the lipid. In the case that the lipid contribution to k_c dominates, the spontaneous curvature scales directly with L, the length of the polymer brush (see also Ref. [21]). The dependence on the polymer-lipid parameters is then given explicitly by Eq. (36). The presence of the polymer strongly favours bending, in a way that depends quadratically on the polymer length and on the $(m_F + 4/3)$ power of the polymer-lipid density. The sign of c_o indicates the preference of the polymer brush for the outside of the lipid aggregate. Eq. (36) is the value for a monolayer. For a bilayer membrane, the spontaneous curvature is zero by symmetry. Nevertheless, the monolayer value of c_o is important for bilayers because it expresses the spontaneous tendency to form micelles [18,33].

When k_c is dominated by the polymer contribution, given by Eq. (34), the spontaneous curvature becomes:

$$c_o = \frac{1}{2(m_F+1)} \frac{1}{L} = \left[2(m_F+1) a_m^{2m_F} n_p \left(\frac{X_p}{A_l}\right)^{1/3}\right]^{-1} \tag{37}$$

The spontaneous curvature then scales inversely with L. Spontaneous bending is less favoured than in the "dilute" case because of the stronger dependence of k_c^p on polymer length and density. Note, however, that it is the product $k_c c_o^2$ (see Eq. (28)) that determines the free energy associated with the spontaneous tendency of the lamellar membrane to bend. More detailed predictions of the spontaneous curvature can be found in Ref. [19].

5. Micelle formation by polymer-lipids

Dispersed alone in water, lipids with hydrophilic polymer headgroups form normal (i.e. oil-in-water) micelles. This is a result of the steric bulk of the polar headgroup chains that is augmented for PEG-linked phospholipids by the electrostatic charge of the lipid phosphate group. When mixed with bilayer-forming lipids, the polymer-lipids therefore have a tendency, which increases with increasing polymer-lipid content, to induce micelle formation in aqueous dispersion.

At lower polymer lipid contents, this can affect both the morphology and permeability of the membrane vesicles. At higher polymer-lipid contents this leads to a broad range of coexistence of micelles and bilayer membranes that has been investigated by several groups [10,34–36]. Two main physicochemical aspects are of relevance: the thermodynamics of the bilayer–micelle coexistence and the scaling of these properties with polymer lipid length. These are dealt with below.

5.1. Bilayer–micelle transition

The extended region of bilayer–micelle coexistence that is found on increasing the concentration of polymer lipid may be described in terms of equilibrium thermodynamics [5,36]. The principal features of the bilayer–micelle transition can then be predicted from the Gibbs phase rule. For a system of two components, polymer and non-polymer lipid with water in excess (i.e. $C=2$), the number of degrees of freedom of the two coexisting phases, bilayer and micellar (i.e. $P=2$), is $F=C-P+1=1$, at constant pressure. At a fixed temperature, the compositions of the interconverting bilayer and micellar phases must therefore remain constant throughout the transition. Direct experimental evidence for this prediction is given by measurements of the rotational freedom of spin-labelled lipid chains in the lamellar component throughout the coexistence region (see Fig. 6). From the outer hyperfine splitting, $2A_{max}$, in the spin-label EPR spectrum, the chain mobility is found to remain constant with increasing total PEG-lipid content, as is expected if the composition of the lamellar phase remains unchanged. An increase in chain rotational mobility (i.e. decrease in A_{max}) is

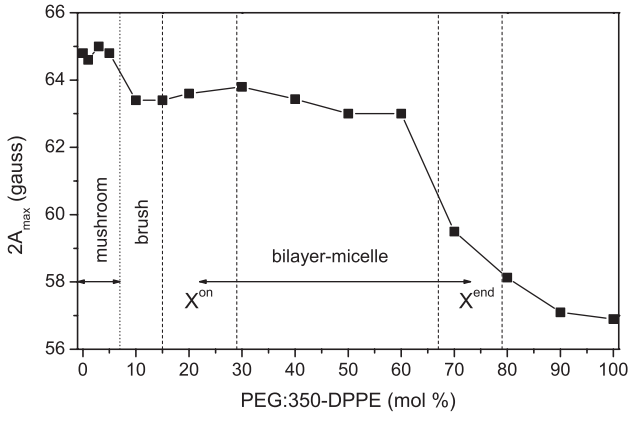

Fig. 6. Dependence of $2A_{max}$, the maximum hyperfine splitting (i.e. restriction of rotational mobility) of spin-labelled phosphatidylcholine (5-PCSL) chains on PEG-lipid content in dipalmitoyl phosphatidylcholine/*N*-PEG:350-dipalmitoyl phosphatidylethanolamine mixed lipid dispersions at 10 °C [10]. The (constant) high values of A_{max} in the bilayer–micelle coexistence region are characteristic of the lamellar gel phase. The vertical dashed lines represent the approximate boundaries of the coexistence region (cf. Fig. 7 upper panel). The initial drop at low PEG-lipid content corresponds to transition from the mushroom to the brush regime (vertical dotted line). The large discontinuity at high PEG-lipid contents is characteristic of the higher chain mobility in the micellar phases.

first observed close to the end of the coexistence region, when the bilayer component has become very small and can no longer be resolved (see also Ref. [10]).

The composition of the bilayer phase is specified by the mole fraction of polymer lipid, X_p^{on}, at the onset of the transition. That at completion of the transition, X_p^{end}, likewise specifies the composition of the micellar phase. The total mole fraction of polymer lipid, X_p, may be expressed in terms of the (constant) compositions, X_p^{on} and X_p^{end}, of the individual phases by means of the conservation of matter:

$$X_p = [1 - f_{tot}\ (\text{micelle})]X_p^{on} + f_{tot}\ (\text{micelle})X_p^{end} \tag{38}$$

where f_{tot} (micelle) is the fraction of total lipid, polymer plus non-polymer, that is in the micellar phase. The degree of conversion to micelles at total mole fraction of polymer lipid, X_p, is therefore given by:

$$f_{tot}\ (\text{micelle}) = \frac{X_p - X_p^{on}}{X_p^{end} - X_p^{on}} \tag{39}$$

It will be noted that this corresponds to the lever rule that is familiar from the phase diagrams of binary mixtures (see, e.g. Ref. [21]). This predicts that the degree of micellar conversion depends linearly on the mole fraction of polymer lipid, within the transition region.

The degree of micellar occupancy of the individual lipid species, polymer (viz., f_p) and non-polymer (viz., f_o), is also of interest. These are quantities that frequently are accessible experimentally. Within the micellar phase, the mole fraction of polymer lipid is X_p^{end}. For the whole sample, the mole fraction of polymer lipid in the micellar phase is therefore $X_p^{end} f_{tot}$ (micelle), i.e. when referred to both phases, where the total mole fraction of polymer lipid is X_p. Therefore, the fraction of polymer lipid that is in the micellar phase is given by:

$$f_p\ (\text{micelle}) = \frac{X_p^{end}}{X_p} f_{tot}\ (\text{micelle}) \tag{40}$$

where f_{tot} (micelle) is given by Eq. (39). Correspondingly, the fraction of non-polymer lipid in the micellar phase is given by:

$$f_o\ (\text{micelle}) = \frac{1 - X_p^{end}}{1 - X_p} f_{tot}\ (\text{micelle}) \tag{41}$$

The dependences of the degrees of micellar occupation on total mole fraction of polymer lipid are given in the lower panel of Fig. 7, for total lipid, and for polymer lipid and non-polymer lipid. These values are deduced from Eqs. (39), (40) and (41), respectively, and a normalised *x*-axis is used. On initiation of the transition at $X_p = X_p^{on}$, the polymer lipid migrates rapidly into the micellar phase, whereas the non-polymer lipid remains preferentially in the lamellar phase. Only towards the end of the transition, specified by

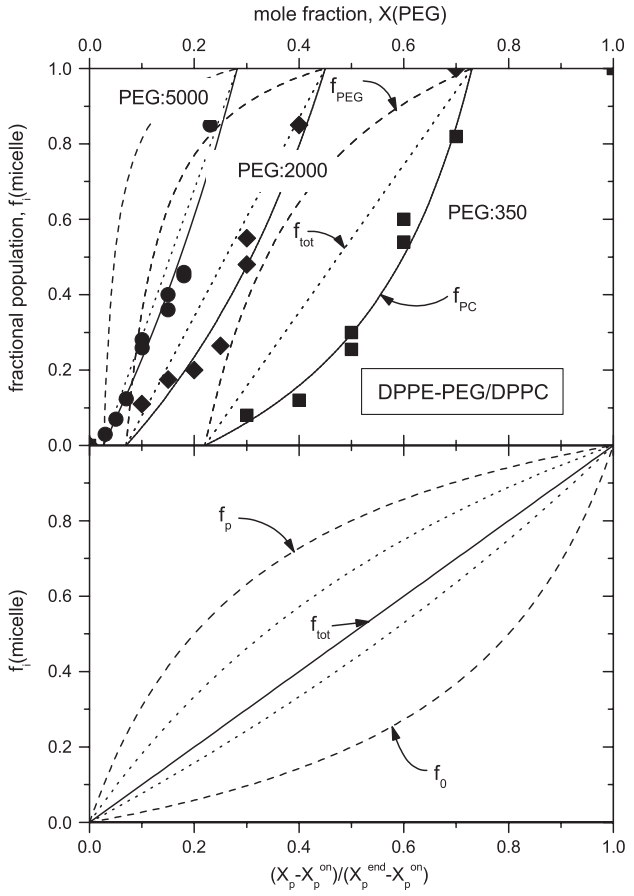

Fig. 7. Lower panel: dependence of the degree of conversion to micelles (f_{tot}, solid line), and the fractional populations of polymer lipid (f_p) and non-polymer lipid (f_o) in the micellar phase (dashed and dotted lines), on the total mole fraction of polymer lipid, X_p. Values are calculated from Eqs. (39)–(41), with $X_p^{end}/X_p^{on}=2$ (dotted lines), 4 (dashed lines) for f_p and f_o, and additionally $X_p^{on}=0.2$ (for f_o). Upper panel: dependence of the degree of conversion to micelles (f_{tot}, dotted lines), and the fraction of PEG-lipid (f_{PEG}) and zwitterionic lipid (f_{PC}) in the micellar phase (dashed and solid lines, respectively), on the total mole fraction of PEG-lipid, X(PEG), in fully hydrated dipalmitoyl phosphatidylcholine/*N*-PEG dipalmitoyl phosphatidylethanolamine mixtures. The left-hand, centre and right-hand sections refer to PEG-lipids with mean polymer molecular weights of 5000 Da (PEG:5000), 2000 Da (PEG:2000) and 350 Da (PEG:350), respectively. The data points correspond to the fraction of spin-labelled phosphatidylcholine in micelles for the mixtures with PEG:2000 (♦) and PEG:350 (■) lipids [36], and with PEG:5000 (●) lipid [10]. The fitting parameters in Eqs. (39)–(41) are: $X_{PEG}^{on}=0.03$, $X_{PEG}^{end}=0.28$ for PEG:5000; $X_{PEG}^{on}=0.07$, $X_{PEG}^{end}=0.45$ for PEG:2000; and $X_{PEG}^{on}=0.22$, $X_{PEG}^{end}=0.73$ for PEG:350 lipids.

$X_p=X_p^{end}$, does the non-polymer lipid migrate more rapidly into the micellar phase.

5.2. Experimental application

Spin-labelled phosphatidylcholine lipid at probe amounts has been used to study micelle formation in fully hydrated mixtures of dipalmitoyl phosphatidylcholine with PEG-linked dipalmitoyl phosphatidylethanolamine of different polymer sizes by using ESR spectroscopy [10,36]. The fraction, f_{PC}, of spin-labelled lipid in micelles was determined by spectral subtraction with mixtures at a temperature for which the lamellar population was in a gel phase and therefore was well resolved spectrally from the more fluid micellar population. The spin-label results for mixtures containing the different chain length PEG-lipids are given in the upper panel of Fig. 7. Fitting Eqs. (39) and (41) to the data yields the lines shown for f_{PC} in Fig. 7 (upper panel), with the fitting parameters given in the figure legend. Use of Eqs. (39) and (40) then allows prediction of the total fraction of micelles (f_{tot}) and fraction of micellar PEG-lipid (f_{PEG}). These are given by the lines without data points, in Fig. 7 (upper panel), for the different mixtures.

The effect of the size of the polymer-lipid headgroup is seen clearly in Fig. 7 (upper panel). This is consistent with considerations of the molecular shape that determines the lipid packing parameter, v/Al, where v is the hydrocarbon chain volume, A is the headgroup area per lipid and l is the effective length of the hydrophobic tail (see, e.g. Refs. [20,33,37]). For PC, $v/Al \approx 1$; for PEG:350 $v/Al<1$ and for PEG:2000 and PEG:5000 the packing parameter is progressively smaller than for PEG:350. Accordingly, micellisation is induced more readily by PEG:2000 ($X_{PEG}^{on}=0.07$) than by the shorter polymer lipid PEG:350 ($X_{PEG}^{on}=0.22$) and yet more readily by PEG:5000 ($X_{PEG}^{on}=0.03$). In addition, the micelles contain a considerably smaller fraction of the PEG:2000 polymer lipid than of the PEG:350 lipid and a yet smaller fraction of PEG:5000 lipid. Throughout the lamellar–micelle transition, the micelles respectively contain a mole fraction $X_{PEG}^{end}=0.28$ of PEG:5000 lipid, $X_{PEG}^{end}=0.45$ of PEG:2000 lipid and $X_{PEG}^{end}=0.73$ of PEG:350 lipid (see Fig. 7, upper panel).

Other methods have also been used to study the degree of micellisation. These results are collected together in Table 2. Indirect measurements using the chain-melting transition behaviour in differential scanning calorimetry were analysed to yield the fraction of PEG-lipid in micelles [34]. Direct measurements of the total lipid in the micellar state were made using high-resolution proton NMR spectroscopy [35]. The values of X_{PEG}^{on} and X_{PEG}^{end} obtained by fitting the data from the two different types of experiments to Eqs. (39) and (40), and to Eq. (41), respectively, are given

Table 2
Values of the parameters X_{PEG}^{on} and X_{PEG}^{end} governing the lamellar–micelle transition obtained from fitting f(micellar) with Eqs. (39)–(41), for different systems containing PEG-lipids

	X_{PEG}^{on}	X_{PEG}^{end}	Reference
DPPC:			
diC_{16} PEG:350	0.22 ± 0.07	0.73 ± 0.06	[36]
diC_{16} PEG:2000	0.07 ± 0.03	0.45 ± 0.05	[36]
diC_{16} PEG:5000	0.03 ± 0.01	0.28 ± 0.01	[10]
diC_{18} PEG-2000	0.05	0.20 ± 0.01	[34]
diC_{18} PEG-5000	0.025	0.14 ± 0.02	[34]
egg PC/POPE 9:1 mol/mol:			
1-C16-2-C18:1-PEG:5000	0.05 ± 0.01	0.33 ± 0.05	[35]

in Table 2. It should be noted that a fixed value was assumed for X_{PEG}^{on} to obtain *f*(micellar) from the calorimetric data [34]. The NMR experiments extended only to $X_{PEG}=0.13$ in the coexistence region [35]. Therefore, the value of X_{PEG}^{end} in this case represents a considerable (linear) extrapolation for f_{tot}.

It is of interest to compare these experimental values with the theoretical calculations using methods of polymer physics that were performed by Hristova and Needham [5]. For PEG:2000, they predict a value of $X_{PEG}^{on}=0.07$ for the onset of micellisation, which is similar to the values given in Table 2. The predicted value for completion of the lamellar–micelle transition is $X_{PEG}^{end}=0.24$, which is intermediate between the values given for PEG:2000 in Table 2. The values calculated theoretically are found to be rather similar in the gel and fluid phases. For PEG:5000, values of $X_{PEG}^{on}=0.035$ and $X_{PEG}^{end}=0.14$ predicted by the Hristova–Needham model are quoted by Baekmark et al. [34]. These values are in reasonable agreement with the data reported by the latter authors (see Table 2), but the value of X_{PEG}^{end} differs considerably from the more direct measurements by Rex et al. [35] and Montesano et al. [10].

5.3. Scaling with polymer length

From Table 2, it can be seen that the mole fraction of polymer lipid, X_p^{on}, required for onset of micellisation depends rather strongly on the polymer length, n_p, as might be expected. The scaling with n_p can be predicted if it is assumed that onset of micellisation takes place at some fixed critical expansion, ΔA_{crit}, of the membrane area by the polymer lipid. Justification for this assumption comes from experiments with spin-labelled lipids which show that onset of micellisation occurs at approximately the same lipid packing density for PEG-lipids of different polymer chain lengths [10]. It is then seen immediately from Eq. (17) that the dependence of X_p^{on} on polymer chain length is given by $X_p^{on} \sim n_p^{-1/(m_F+1)}$. The value of the exponent is therefore $-3/5$ in mean field theory and $-6/11$ in scaling theory. For PEG-lipids with $n_p=8$, 45 and 114, it is found experimentally that the exponent of n_p is -0.74 ± 0.06 [10]; a value of -0.7 ± 0.1 is obtained from the combined values in Table 2. This is similar to the theoretical predictions and closer to that from mean-field theory, although still somewhat greater than the latter. A similar scaling has been predicted for the saturation level of polymer lipid in the bilayer by equating the repulsive pressure in the polymer brush with the maximum tensile stress that a lipid bilayer membrane can support [23]. The predicted saturation values were, however, higher than the polymer lipid content at the onset of micellisation.

In contrast, the mole fraction of polymer lipid, X_p^{end}, at the end of the lamellar–micellar transition has a considerably weaker dependence on n_p than does X_p^{on} (see Table 2). This is because X_p^{end} depends more strongly on the properties of the micelles than does X_p^{on}. For PEG-lipids, a consistent interpretation of the experimental values has been given in terms of the different surface area per lipid in bilayers and micelles and the different area expansions induced by the polymer lipids in these two states [10].

6. Membrane–membrane interactions

The interaction forces between polymer-grafted lipid surfaces are of direct relevance to their function in steric stabilisation of liposomes. Consequently, they have been the subject of several detailed experimental studies [6,7,17,38]. The experimental approaches used include the surface force apparatus, X-ray diffraction measurements under osmotic stress, and micromechanical manipulation of giant lipid vesicles. Two different regimes of grafting density can be distinguished, viz., those corresponding to the mushroom and brush regimes (see Fig. 8). In the dilute mushroom regime, Hristova and Needham [23] propose a mean-field treatment based on the Flory approach at low compression, and adopt the scaling theory of De Gennes and Alexander in the high-compression regime. In the higher concentration brush regime, both the scaling and mean-field approaches already introduced apply (see Ref. [23]). A simple random-flight model, first introduced by Dolan and Edwards [39], has also been considered in the very high dilution regime.

6.1. Random flight model

The random flight approach of Dolan and Edwards [39] uses the diffusion equation, neglects excluded volume effects, and thus can only be expected to apply to reasonably long polymers at high dilution. It is included here because of the success in interpreting surface-force measurements on polymer-grafted lipids at low surface coverage [17].

A random flight polymer chain is confined between two plane surfaces distance d apart. Solution of the diffusion equation with the boundary condition that the probability of finding a chain segment goes to zero at the confining surfaces, gives the required configurational distribution. Then, by integrating over space, the total number of configurations that are confined between the two planes, relative to that for the free polymer, is [39]:

$$\Omega(n_p,d)=1-2\exp(-3d^2/2n_pa_m^2) \tag{42}$$

for $d^2/n_pa_m^2>1.1$, or:

$$\Omega(n_p,d)=\sqrt{\frac{8\pi n_p}{3}}\frac{a_m}{d}\exp\left(\frac{-\pi^2 n_p a_m^2}{6d^2}\right) \tag{43}$$

for $d^2/n_pa_m^2<2.8$. In Eqs. (42) and (43), n_p is the number of polymer segments, as usual, and a_m is the segment

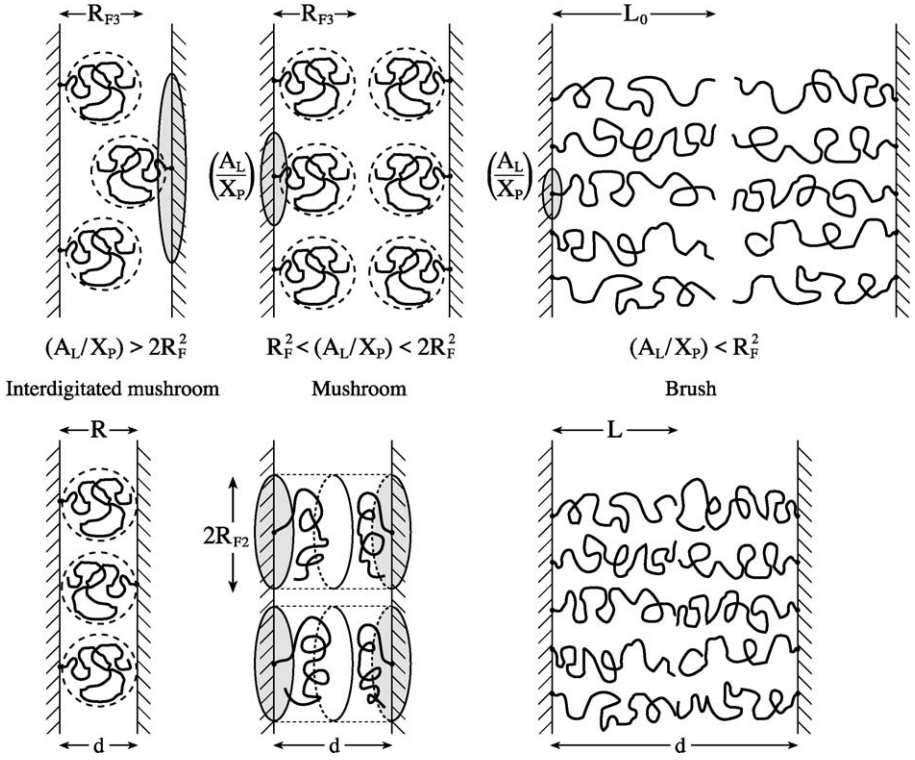

Fig. 8. Schematic representation of the different regimes of polymer grafting density, X_p/A_l, for interacting membrane surfaces (see Ref. [7]). Upper row: in the relaxed state; lower row: under compression. R_{F3} is the Flory radius of an uncompressed mushroom; R_{F2} is the radius of the flattened mushroom; L_o is the length of the polymer brush.

length. The free energy of interaction ($F_R = -k_BT\ln\Omega$) is then [39]:

$$F_R(d)/k_BT \approx -\left[\frac{\pi^2 n_p a_m^2}{6d^2} + \ln\left(\sqrt{\frac{3}{8\pi n_p}}\frac{d}{a_m}\right)\right] \quad (44)$$

for $d^2/n_p a_m^2 \le 3$, or:

$$F_R(d)/k_BT \approx -2\exp\left(\frac{-3d^2}{2n_p a_m^2}\right) \quad (45)$$

for $d^2/n_p a_m^2 \ge 3$.

The interbilayer repulsive pressure, $P_R = -(X_p/A_l)\partial F_R/\partial d$, where X_p is the mole fraction of polymer-grafted lipid and A_l is the area per lipid molecule, is then finally given by:

$$P_R(d)/k_BT \approx \left(\frac{X_p}{A_l}\right)\left[\frac{-\pi^2 n_p a_m^2}{3d^3} + \frac{1}{d}\right] \quad (46)$$

for $d^2/n_p a_m^2 \le 3$, or:

$$P_R(d)/k_BT \approx -6\left(\frac{X_p}{A_l}\right)\frac{d}{n_p a_m^2}\exp\left(\frac{-3d^2}{2n_p a_m^2}\right) \quad (47)$$

for $d^2/n_p a_m^2 \ge 3$.

6.2. Mushroom regime

Two regions of polymer grafting density can be distinguished within the mushroom regime as indicated schematically in Fig. 8. At low polymer concentrations, the mushrooms from opposing membranes are able to interdigitate on compression [7]. Each mushroom is then compressed against both membrane surfaces (left-hand panel of Fig. 8). At higher polymer concentrations, the mushrooms from opposing membranes do not interdigitate and are compressed against one another (centre panel of Fig. 8). At low compression, the mushrooms maintain their approximately spherical shape (Fig. 8, left lower panel). At high compression, the mushrooms distort to flattened discs (Fig. 8, centre lower panel).

6.2.1. Low compression

For low compression, i.e. little elastic distortion of the mushrooms, Hristova and Needham [23] use the Flory mean-field approach already introduced in connection with the mushroom regime. From a somewhat more general form of Eq. (1), the free energy per polymer mushroom is given by:

$$F_p(R)/k_BT \approx \left(\frac{R_{F3}^o}{a_m}\right)^{1/3}\left[\frac{2}{3}\left(\frac{R_{F3}^o}{R}\right)^3 + \left(\frac{R}{R_{F3}^o}\right)^2\right] \quad (48)$$

where the equilibrium value of R for noncompressed mushrooms is given by:

$$R_{F3}^o = (3k/2)^{1/5}R_{F3} = (3k/2)^{1/5}a_m n_p^{3/5} \quad (49)$$

where k is a multiplicative factor that scales the excluded volume term relative to the stretching term in Eq. (1), and R_{F3} is the conventional Flory radius given by Eq. (2). The force per unit area exerted on compressing the mushroom, $P^{MF} = -(X_p/A_l)\partial F_p/\partial R$, is hence given from Eq. (48) by:

$$P^{MF}(R)/k_BT \approx (a_m R_{F3}^{o2})^{-1/3}\left(\frac{X_p}{A_l}\right)\left[\left(\frac{R_{F3}^o}{R}\right)^4 - \left(\frac{R}{R_{F3}^o}\right)\right] \quad (50)$$

In the very low-density regime, $A_l/X_p > 2\pi R_{F3}^2$, the mushrooms from opposing membranes interdigitate without mutual interaction (see left-hand panel of Fig. 8). The pressure exerted between the mushrooms is then given by Eq. (50) with $R = d$, for membrane–membrane separations $d < R_{F3}$, i.e. less than the size of a single mushroom. In the intermediate density regime, $2\pi R_{F3}^2 > A_l/X_p > \pi R_{F3}^2$, the mushrooms on opposing membranes first come into contact at $d \sim 2R_{F3}$ and the pressure exerted between the membranes is then given by Eq. (50), with $R = d/2$ [23]. The dashed line in the upper panel of Fig. 9 gives the dependence of the bilayer–bilayer pressure on intermembrane separation, i.e. as a function of $R = d/2$, for $k \approx 1$.

6.2.2. High compression

The scaling laws introduced by Daoud and De Gennes [15] allow treatment of systems at high compression, where the mushrooms no longer are three-dimensional but become two-dimensional flattened pancakes of Flory radius:

$$R_{F2} \approx a_m n_p^{3/4} \quad (51)$$

which is the two-dimensional equivalent of Eq. (2) for R_{F3}, where $\nu = 3/4$ from Eq. (3) (see Fig. 8, centre panel). The corresponding scaling law for R_{F2} is [15]:

$$R_{F2} \approx R_{F3} \times (R_{F3}/d)^{m_R'} \quad (52)$$

Hence, from Eq. (2) for R_{F3}, correspondence of the dependence of R_{F2} on n_p in Eq. (52) with that in Eq. (51) requires that $m_R' = 1/4$. The scaling law for the radius of a strongly compressed mushroom is therefore:

$$R_{F2} \approx a_m\left(\frac{a_m}{d}\right)^{1/4} n_p^{3/4} \quad (53)$$

Compression becomes sufficient for the mushrooms to overlap when $R_{F2}^2 \sim A_l/X_p$, which occurs at the critical membrane separation:

$$d_{crit} \approx a_m\left(\frac{a_m^2}{A_l}\right)^2 X_p^2 n_p^3 \quad (54)$$

At this point, not only elastic forces arising from compression of the mushrooms, but also osmotic forces arising from overlap of the mushrooms, contribute to the repulsive intermembrane pressure [23].

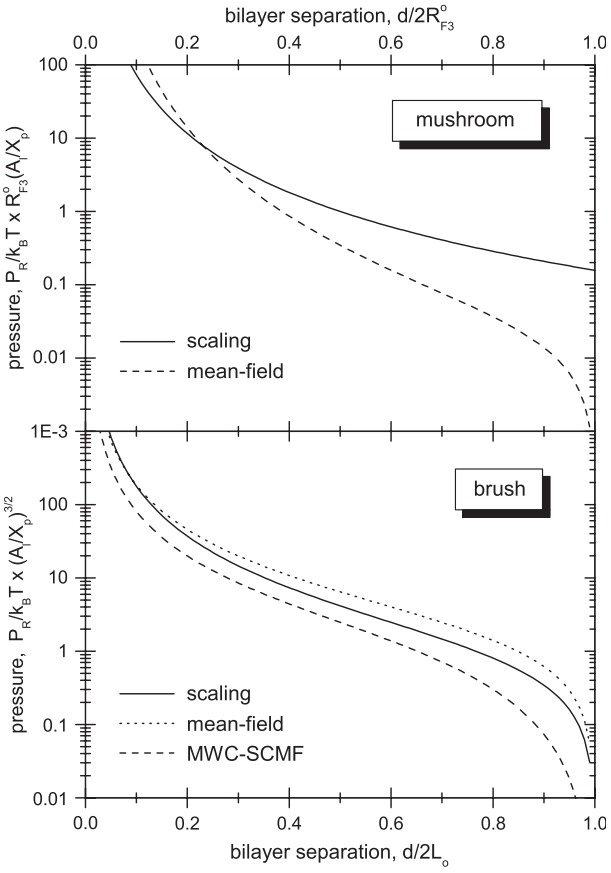

Fig. 9. Bilayer–bilayer repulsive pressure, P_R, as a function of interbilayer separation, d, for polymer grafted membranes. Upper panel: in the mushroom regime. The bilayer spacing is normalised to the Flory radius, R_{F3}^o, of the polymer that is given by Eq. (49) with $k = 1$. Solid line is the result from Alexander–De Gennes scaling theory according to Eq. (57). Dashed line is the mean-field result according to Eq. (50). The dimensionless ordinate and abscissa apply quite generally for scaling theory. For mean-field theory, the polymer length is taken as $n_p = 45$; and the ordinate values increase with increasing n_p. Lower panel: in the brush regime. The bilayer spacing is normalised to the height, L_o, of the uncompressed polymer brush that is given by Eq. (60) or (66), i.e. $L_o = L_o^{MF}$ or L_o^{SC}. Solid line is the result from Alexander–De Gennes scaling theory according to Eq. (67). Dotted line is the mean-field theory result according to Eq. (61). Dashed line is the Milner–Witten–Cates SCMF theory result according to Eq. (64), with the explicit numerical prefactor and $L_o = L^{MWC}$. The dimensionless ordinate and abscissa apply quite generally for scaling theory. For the mean-field theories, the ordinate is calculated for a polymer-lipid content $X_p = 0.1$, with $A_l = 0.6$ nm^2 and $a_m = 0.39$ nm; and the ordinate-value decreases with increasing (X_p/A_l).

The scaling law for the configurational free energy of the compressed mushroom is [15]:

$$F_p^{SC}/k_BT \approx (R_{F3}/d)^{m_F'} \quad (55)$$

From Eq. (2) for R_{F3} and the usual requirement that the free energy is extensive in n_p, one gets $m_F' = 5/3$. Thus Eq. (55) becomes:

$$F_p^{SC}(d)/k_BT \approx n_p(a_m/d)^{5/3} \quad (56)$$

for the dependence of the polymer configurational free energy on membrane separation. The conformational contribution to the intermembrane pressure, $P_R = -(X_p/A_l)\partial F_p/\partial d$, is then:

$$P_R^{SC}/k_BT \approx \frac{n_p}{a_m}\left(\frac{X_p}{A_l}\right)\left(\frac{a_m}{d}\right)^{8/3} \quad (57)$$

This is the total pressure for separations greater than the critical value for overlap of the compressed mushrooms, i.e. for $d>d_{crit}$. This scaling theory estimate of the repulsive pressure in the high-compression regime is shown by the solid line in the upper panel of Fig. 9.

For stronger compression, $d<d_{crit}$, the osmotic contribution must be added to Eq. (57). For the latter, Daoud and De Gennes [15] obtain the following (see, e.g. Ref. [23]):

$$P_R^{osm}/k_BT \approx n_p^3 a_m^5\left(\frac{X_p}{A_l}\right)^3\left(\frac{2}{d}\right)^2 \quad (58)$$

This corresponds to the osmotic pressure of highly compressed, overlapping polymer chains with two-dimensional behaviour.

6.3. Brush regime

As for the treatment of the properties of single bilayers in the brush regime that were given previously, bilayer–bilayer interactions of polymer-grafted membranes are discussed in terms of mean-field theory and of scaling theory. The situation in the brush regime is indicated schematically in the right-hand panel of Fig. 8.

6.3.1. Mean-field theory

The dependence of the polymer free energy on the height, L, of the polymer brush is given by Eq. (5), where $L \equiv R = d/2$, i.e. half the bilayer separation. From a more general form of Eq. (5) we get:

$$F_p^{MF}(d)/k_BT \approx a_m^{1/3} L_o^{MF}\left(\frac{X_p}{A_l}\right)^{1/3}\left[\frac{L_o^{MF}}{L}+\frac{1}{2}\left(\frac{L}{L_o^{MF}}\right)^2\right] \quad (59)$$

where it is assumed (as previously) that $v_m \approx a_m^3$. The equilibrium length of the polymer brush, L_o^{MF}, for the isolated membrane is given by:

$$L_o^{MF} = (k/2)^{1/3} L^{MF} = (k/2)^{1/3} n_p a_m^{5/3} (X_p/A_l)^{1/3} \quad (60)$$

where L^{MF} is given by Eq. (6) and k is a multiplicative factor that represents the relative strength of the excluded volume and stretching terms (first and second on the right) in Eq. (5). The repulsive pressure between bilayers $P_R = -(X_p/A_l)(\partial F_p^{MF}/\partial L)$ is therefore given by:

$$P_R^{MF}(d)/k_BT \approx a_m^{-1/3}\left(\frac{X_p}{A_l}\right)^{4/3}\left[\left(\frac{2L_o^{MF}}{d}\right)^2-\left(\frac{d}{2L_o^{MF}}\right)\right] \quad (61)$$

The dotted line in the lower panel of Fig. 9 gives the dependence of the bilayer–bilayer repulsive pressure on the intermembrane separation, d, according to Eq. (61).

In the SCMF theory of Milner et al. [12,13], the distribution of polymer chain ends is parabolic rather than the step function that is implicitly assumed in the simple mean-field theory based on Eq. (5). For this model, the dependence of the polymer free energy on height, L, of the polymer brush contains an additional term, compared to Eq. (59) [13]:

$$F_p^{MWC}(R)/k_BT = \left(\frac{\pi^2}{96}\right)^{1/3} n_p a_m^{4/3}\left(\frac{X_p}{A_l}\right)^{2/3} \times\left[\frac{L^{MWC}}{L}+\left(\frac{L}{L^{MWC}}\right)^2-\frac{1}{5}\left(\frac{L}{L^{MWC}}\right)^5\right] \quad (62)$$

where the maximum extent of the polymer brush is given by:

$$L^{MWC} = \left(\frac{12}{\pi^2}\right)^{1/3} n_p a_m^{5/3}\left(\frac{X_p}{A_l}\right)^{1/3} \quad (63)$$

As noted previously, with these explicit premultiplying factors, the self-consistent mean-field (MWC) results are exact. The bilayer–bilayer repulsive pressure, $P_R = -(X_p/A_l)(\partial F_p/\partial L)$, with $L = d/2$ is then given by (see Ref. [23]):

$$P_R^{MWC}(d)/k_BT = \frac{1}{2}\left(\frac{\pi^2}{12}\right)^{2/3} a_m^{-1/3}\left(\frac{X_p}{A_l}\right)^{4/3}\left[\left(\frac{2L^{MWC}}{d}\right)^2 - 2\left(\frac{d}{2L^{MWC}}\right)+\left(\frac{d}{2L^{MWC}}\right)^4\right] \quad (64)$$

The lower panel of Fig. 9 compares the predicted dependence of the repulsive pressure on interbilayer distance, d, for the two mean-field models. The values for the SCMF theory are lower than those given for the simple mean-field theory, partly because the explicit prefactor of $1/2(\pi^2/12)^{2/3} = 0.439$ has been included for the former. The repulsive pressure goes to zero at a greater value of $d/2L_o^{MF}$ for the SCMF model than for the MF model, because L^{MWC} is $2(3/\pi^2)^{1/3} = 1.34$ times greater than L_o^{MF} with $k = 1$ (compare Eqs. (60) and (63)). As stated previously, the polymer brush region has a step profile with length L_o^{MF} in the simple mean-field approach, but has a parabolic profile with maximum extent L^{MWC} in the SCMF model.

6.3.2. Scaling theory

The free energy of the polymer brush, F_p^{SC}, for an isolated membrane that was given in Eq. (12) corresponds to the equilibrium energy of the uncompressed chains, and does not include explicitly the separate contributions from the repulsive energy and the elastic stretching energy in a compressed polymer brush of height, L. Scaling laws for the free energy in this latter case have been given by Alexander [3]:

$$F_p^{SC}(L)k_BT \approx L_o^{SC}\left(\frac{X_p}{A_l}\right)^{1/2}\left[\frac{7}{5}\left(\frac{L_o^{SC}}{L}\right)^{5/4}+\left(\frac{L}{L_o^{SC}}\right)^{7/4}\right] \quad (65)$$

where the first term is the De Gennes steric repulsion energy in the brush and the second term is the elastic energy for compression of the brush (see also Ref. [40]). The equilibrium length of the uncompressed polymer brush, L_o^{SC}, in Eq. (65) is given by:

$$L_o^{SC} = \left(\frac{5k}{7}\right)^{1/3} L^{SC} = \left(\frac{5k}{7}\right)^{1/3} n_p a_m^{5/3}\left(\frac{X_p}{A_l}\right)^{1/3} \quad (66)$$

where k is a multiplicative factor that represents the relative strength of the excluded volume and stretching terms in Eq. (65). The repulsive pressure between bilayers $P_R = -(X_p/A_l)\partial F_p^{SC}/\partial L$ is therefore given from Eq. (65) (for $L = d/2$) by [23]:

$$P_R^{SC}(d)/k_BT \approx \left(\frac{X_p}{A_l}\right)^{3/2}\left[\left(\frac{2L_o^{SC}}{d}\right)^{9/4}-\left(\frac{d}{2L_o^{SC}}\right)^{3/4}\right] \quad (67)$$

It is readily seen from Eq. (67) that the equilibrium situation for an isolated bilayer, viz. $P_R^{SC}(d) = 0$, is given by $d/2 = L_o^{SC}$ and that by substituting $L = L_o^{SC}$ in Eq. (65), the equilibrium free energy is given by Eq. (12) derived above.

The solid line in the lower panel of Fig. 9 gives the dependence of the bilayer–bilayer repulsive pressure on interbilayer spacing according to scaling theory. Here it is compared with the predictions of the two mean-field theories. The latter are given for a polymer-lipid content of $X_p = 0.1$, whereas with the dimensionless variables given in Fig. 9 (lower panel), the results of scaling theory are generally valid for all polymer-lipid contents.

6.4. Experimental applications: surface force measurements

In the surface force apparatus, the ratio of the force, $\mathcal{F}(d)$, between the crossed cylindrical surfaces of radius, R_o, is related to the free energy of interaction, per unit area, between two flat surfaces at the same distance d apart by the Derjaguin approximation [37,41]:

$$\mathcal{F}(d)/R_o = 4\pi[F_p(d/2) - F_p(L_o)](X_p/A_l) \quad (68)$$

where $F_p(d/2)$ is the free energy per polymer in a brush of height $d/2$ and L_o is the height of the unperturbed brush. The interactions between the two membrane-bearing surfaces are therefore obtained directly from the force–distance ($\mathcal{F}$ vs. d) curves.

The interactions between phosphatidylethanolamine (PE) bilayers containing PEG-grafted PE has been studied in the low (~ 1%) and high (~ 5–10%) grafting regimes, by using the surface force apparatus [17]. In the absence of grafted polymer, PE bilayers adhere because of the reduced hydration repulsion, relative to van der Waals' attraction, in comparison with phosphatidylcholine bilayers [21,42]. Fig. 10 gives the force–distance relations for polymer densities in the very dilute mushroom regime. The steep part of the curve at short membrane separations arises predominantly from the direct steric interaction of the polymer with the membrane surface, whereas the more slowly decaying part at large separations arises from electrostatic repulsion that is contributed by the negative charge on the polymer lipid. The solid line in Fig. 10 represents a fit to the Dolan–Edwards theory, with the electrostatic contribution calculated explicitly from double-layer theory. For Dolan–Edwards theory, the ratio of the repulsive force, F, to radius, R_o, is given by [17]:

$$\frac{\mathcal{F}^{DE}(d)}{R_o} = 72\pi\left(\frac{A_l}{X_p}\right)k_BTe^{-d/R_{F3}} \quad (69)$$

where d is the separation of the crossed cylindrical surfaces and R_{F3} is the Flory radius of the random-flight polymer. The surface density of polymer-lipid, X_p/A_l, is determined directly for the monolayers from which Langmuir–Blodgett layers are deposited on the mica surfaces of the force apparatus. The value of $R_{F3} = 3.1$ nm is the only fitted parameter in Fig. 10, and is close to theoretical estimates of the Flory radius ($R_{F3} \approx 3.5$–3.8 nm) for a PEG:2000 polymer.

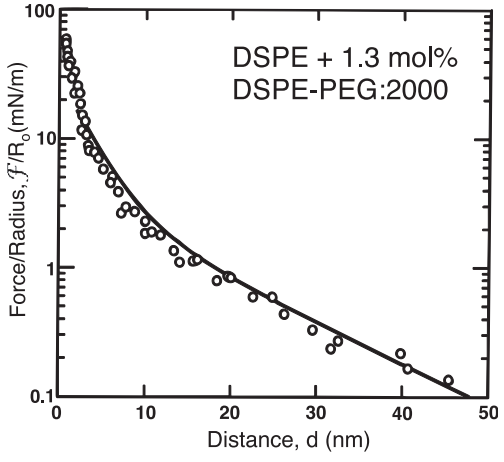

Fig. 10. Force versus separation curves for DSPE bilayers containing 1.3 mol% DSPE-PEG:2000, in the dilute mushroom regime. Solid line is the fit to Dolan–Edwards theory (Eq. (69)) with $(A_l/X_p) = 33$ nm^2, yielding $R_{F3} = 3.1$ nm, together with the electrostatic repulsion calculated from double-layer theory [17].

Fig. 11 gives the force–distance relations for the steric bilayer repulsion, at polymer densities in the brush regime. For separation distances below twice the thickness, L^{SC}, of the polymer brush layer, the force with distance relation for two curved cylindrical surfaces of radius, R_o, is given from Eqs. (65) and (68) for scaling theory by [17]:

$$\frac{\mathcal{F}^{SC}(d)}{R_o} \approx k_B T \left(\frac{X_p}{A_l}\right)^{3/2} L_o^{SC} \left[\frac{7}{5}\left(\frac{2L_o^{SC}}{d}\right)^{5/4} + \left(\frac{d}{2L_o^{SC}}\right)^{7/4} - \frac{12}{5}\right] \tag{70}$$

with $L = d/2$, where L_o^{SC} is given by Eq. (66). The fit of Eq. (70), with adjustable prefactor, which is given in Fig. 11, corresponds to $L_o^{SC} = 5.4$ nm. This is rather close to predictions of Eq. (10) for a PEG:2000 polymer with $n_p = 45$, but less than the value of 6.5–7.0 nm that is determined experimentally for the thickness of the polymer brush.

More recently, Efremova et al. [38] have performed surface force experiments with PE bilayers containing an uncharged, PEG-grafted, two-chain lipid SAPDS (3-stearamidyl-2-(monomethoxyPEG-succinyl)-1-stearoyl-3-aminopropane-1,2-diol). As expected, long-range electrostatic repulsion was absent. Surface forces were repulsive and attributed to osmotic interactions between the polymer chains. The force between PE surfaces bearing 1.3 mol% (mushroom regime) and 4.5 mol% (weak overlap) PEG:2000-lipid extended up to separations ~ 8.5 nm. This is roughly the separation at which the polymer chains cease to interact, and is comparable to twice the Flory radius, R_{F3}, of PEG:2000 (see Eq. (2)). At 10 mol% PEG:2000-lipid, steric repulsion between the two dense polymer brushes was found to begin at separations below ~ 12 nm. This results from the more extended conformation of the polymer chains in the brush regime. These findings are consistent with those for the non-electrostatic component of the repulsion between PE surfaces containing negatively charged DSPE-PEG:2000 that were described above.

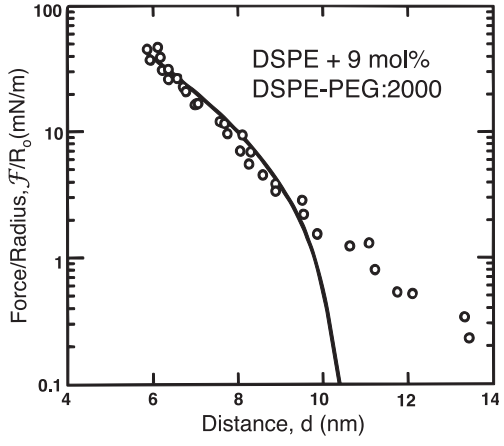

Fig. 11. Force versus separation curves for DSPE bilayers containing 9 mol% DSPE-PEG:2000 in the brush regime. The contribution from electrostatic repulsion has been subtracted by extrapolation of the data at larger separations. Solid line is the fit to polymer scaling theory (Eq. (70)) yielding $L^{SC} = 5.4$ nm [17].

For 1.5 mol% of the neutral PEG:2000 lipid in the mushroom regime, the force–distance relation was well described by Eq. (69), with an adjustable prefactor and a value of $R_{F3} = 2.9 \pm 0.1$ nm. This is close to that obtained for negatively charged DSPE-PEG:2000, also in the mushroom regime [17]. For 4.5 and 10 mol% of the neutral PEG:2000 lipid, comparably good fits to those of Kuhl et al. [17] for DSPE-PEG:2000 at similar concentrations were found by using the scaling theory expression, Eq. (70), for the brush regime. The fitting parameters were also similar. However, a better description of the interactions between the polymer brushes was obtained by using the SCMF theory of Milner, Witten and Cates (MWC). In the latter treatment, the ratio of force to radius is given from Eqs. (68) and (62) by [38]:

$$\frac{\mathcal{F}^{MWC}(d)}{R_o} = \left(\frac{2\pi^5}{3}\right)^{1/3} n_p a_m^{4/3} \left(\frac{X_p}{A_l}\right)^{5/3} \times \left[\frac{2L^{MWC}}{d} + \left(\frac{d}{2L^{MWC}}\right)^2 - \frac{1}{5}\left(\frac{d}{2L^{MWC}}\right)^5 - \frac{9}{5}\right] \tag{71}$$

where L^{MWC} is given by Eq. (63). Good fits were obtained with values of $L^{MWC} = 5.2 \pm 0.3$ nm for 4.5 mol% PEG-lipid and 6.2 ± 0.3 nm for 10 mol% PEG-lipid. Both these values are in good agreement with the thickness of the polymer brush measured by surface plasmon resonance [38]. For comparison, Eq. (63) with $a_m = 0.39$ nm predicts $L^{MWC} = 4.7$ and 6.1 nm for 4.5 and 10 mol% of PEG:2000-lipid, respectively, where $A_l = 0.43$ nm^2 was measured at the point of Langmuir–Blodgett transfer of the lipid monolayers.

6.5. Experimental applications: osmotic stress experiments

Measurement of the equilibrium separation between opposing bilayers as a function of applied osmotic stress, by using X-ray diffraction, gives the dependence of the bilayer–bilayer repulsive pressure on interbilayer separation. This technique has been used to study the steric repulsion of distearoyl phosphatidylcholine (DSPC) bilayers containing varying concentrations of PEG-lipids of different polymer sizes [7]. The equilibrium bilayer separation decreases monotonically with increasing applied osmotic pressure. Comparison of the experimental pressure–distance curves with the various theoretical models were made.

Fig. 12 gives the pressure–separation curves for DSPC with 1.5 mol% DSPE-PEG:750, which is representative

of the mushroom regime. At high applied pressures ($\log P > 6.5$), the data are well described by the Flory-based mean-field model for fully interdigitated mushrooms according to Eq. (50) (Fig. 12, upper panel). At lower applied pressures ($\log P \leq 6.0$), the model of partially interdigitated mushrooms is required, combined with PEG-molecular weight dispersity (see Fig. 12, lower panel). This model corresponds to a weighted average of fully interdigitated ($R = d$ in Eq. (50)) and non-interdigitated ($R = d/2$) species [7].

Fig. 13 gives the pressure–separation curves for DSPC with 10 mol% of DSPE-PEG:2000, which is representative of the brush regime. There is good agreement between the experimental data and the predictions of the SCMF theory (MWC, Eq. (64)) for applied pressures $5.5 < \log P < 6.0$. Over this range, scaling theory (Eq. (67)) predicts separations that are somewhat larger, by ~ 1 nm. For lower applied pressures, $\log P < 5.5$, the measured interbilayer spacings are up to 3.0 nm larger than predicted for monodisperse polymer chains. The effect of PEG polydispersity is in the correct direction to account for the difference between experimental data and theoretical predictions (see Fig. 13 and Ref. [7]). Further data and discussion can be found in the latter reference.

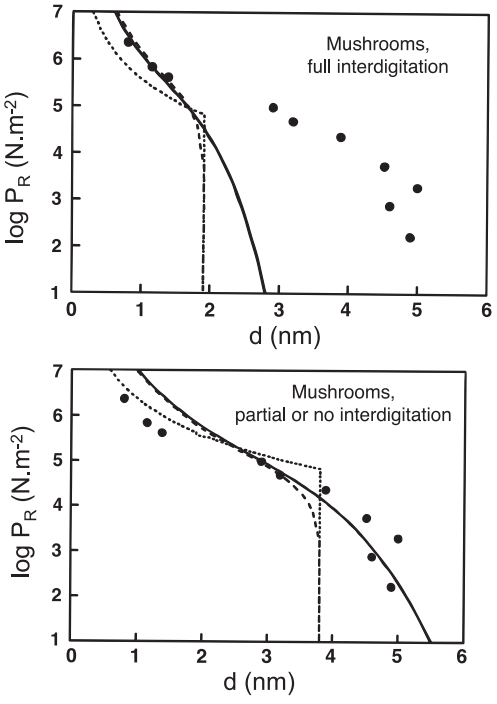

Fig. 12. Dependence of interbilayer separation (d, x-axis) on applied osmotic pressure (P_R, y-axis) for multilamellar dispersions of distearoyl phosphatidylcholine (DSPC) + 1.5 mol% DSPE-PEG:750, in the mushroom regime. Upper panel: Flory-based mean-field predictions for fully interdigitated mushrooms, i.e. Eq. (50) with $R = d$ (dashed line), and similarly for polydisperse Flory mushrooms (solid line); dotted line gives the predictions of scaling theory, i.e. Eq. (57) truncated at $d = R_{F3}$. Lower panel: Flory-based mean-field predictions for partially interdigitated mushrooms (dashed line) and with PEG-molecular weight polydispersity (solid line); and scaling theory predictions for partially interdigitated mushrooms (dotted line) [7].

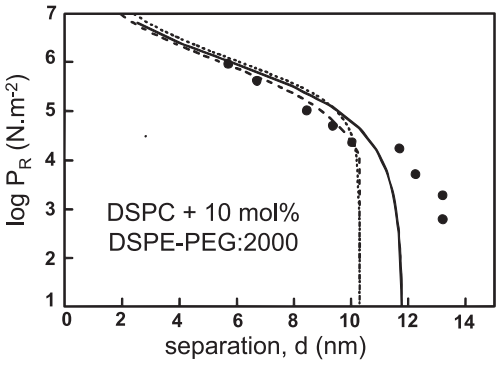

Fig. 13. Dependence of interbilayer separation (d, x-axis) on applied osmotic pressure (P_R, y-axis) for multilamellar dispersions of DSPC + 10 mol% DSPE-PEG:2000, in the brush regime. Dashed line: predictions from SCMF theory (i.e. MWC, Eq. (64)); solid line: MWC with polydispersity of PEG molecular weight; dotted line: scaling theory prediction (i.e. Eq. (67)) [7].

Hansen et al. [16] have shown that the osmotic stress data of Kenworthy et al. [7] for DSPC containing 10 and 20 mol% of the longer polymer lipid DSPE-PEG:5000 can be well described with scaling theory. This success is attributed to the relatively high volume fraction of polymer chains in these samples, hence achieving true semi-dilute—rather than dilute—behaviour (see Section 2.4).

6.6. Experimental applications: adhesion measurements

Micromechanical tests of adhesion between giant phospholipid vesicles containing phospholipids grafted with PEG chains have been performed by Evans et al. [6]. These measurements constitute a direct determination of the steric influence of grafted hydrophilic polymers on the surface interactions of liposomes. Three graft chain lengths ($n_p \approx 45$, 114 and 273) and several surface densities of grafting were employed. These extend from dilute, non-interacting mushrooms to marginal brushes with mean volume fractions up to 0.06. Adhesion was induced by the depletion forces resulting from addition of non-absorbing free polymer. The latter increases the adhesion energy over that of pure van der Waals' attraction by one to two orders of magnitude, when mole fractions of the free polymer reach 0.1–0.2 [43].

At vesicle contact, where the free polymer is excluded, the scale of the adhesion energy is given by the product of the osmotic pressure, Π_f, and the correlation length, ξ_f, of the free polymer in solution, i.e. by $\Pi_f \xi_f$. In the Flory mean-field theory, the osmotic pressure at a volume fraction, ϕ_f, of free polymer is given by [6]:

$$\Pi_f = \frac{k_B T}{a_m^3} v_e \frac{\phi_f^2}{2} \tag{72}$$

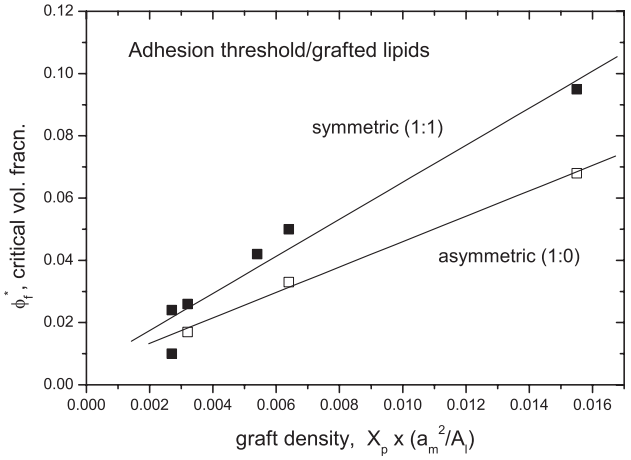

Fig. 14. Adhesion threshold, ϕ_f^*, for the volume fraction of free PEG-polymer in the bathing solutions of giant unilamellar 1-stearoyl-2-oleoyl-phosphatidylcholine vesicles, as a function of the mole fraction, X_p, of PEG-lipid of size $n_p = 114$ or 273 in both vesicles (symmetric), or in only one vesicle (asymmetric), of the adhering partners [6].

where $v_e = 1-2\chi$ is the Flory–Huggins excluded volume parameter. Correspondingly, the correlation length of the free polymer is given by [44]:

$$\xi_f = \frac{a_m}{(6v_e\phi_f)^{1/2}} \tag{73}$$

Hence, the required product depends on volume fraction of free polymer according to $\Pi_f\xi_f \sim \phi_f^{3/2}$. A similar result is obtained from scaling theory, for which $\Pi_f \sim \phi_f^{9/4}$ and $\xi_f \sim 1/\phi_f^{3/4}$ [2].

Fig. 14 gives the dependence of the volume fraction of free polymer, ϕ_f^*, at the onset of vesicle adhesion on mole fraction of PEG-lipid in the vesicles. For long polymers, this depends neither on the length of the free polymer nor on that of the grafted polymer [6]. The linear relation found in Fig. 14 suggests that the steric barrier that must be overcome for adhesion has an energy scale that varies with mole fraction of polymer lipid according to $X_p^{3/2}$, and has a size of the order $\sim k_BT(a_m^2/A_l)\,X_p^{3/2}$. The polymer layers on the two interacting vesicles contribute additively to the steric barrier, because the ratio of slopes in Fig. 14 for symmetric and asymmetric distributions of grafting is $\sim 2^{2/3}$. These results establish a parsimonious criterion for stabilisation of vesicle surfaces grafted with homopolymers [6].

7. Protein adsorption

Protein adsorption assumes a central role in the implementation of steric stabilised liposomes as drug delivery systems. The purpose of the polymer coat is to suppress opsonisation by serum proteins. This prevents recognition by macrophages and clearance from the blood circulation by the reticuloendothelial system.

At low protein concentration, c_{prot}, the adsorption on polymer-grafted lipid membranes is described by the Langmuir adsorption isotherm (see, e.g. Ref. [45]):

$$\theta = K^{ads}c_{prot} \tag{74}$$

where θ is the degree of surface coverage and K^{ads} is the equilibrium constant. Two situations are distinguished, depending on the size, R_{prot}, of the protein, relative to the polymer grafting density, X_p/A_l [46]. For small proteins, $\pi R_{prot}^2 < A_l/X_p$, the protein penetrates the polymer layer and adsorbs to the underlying surface (primary adsorption—see

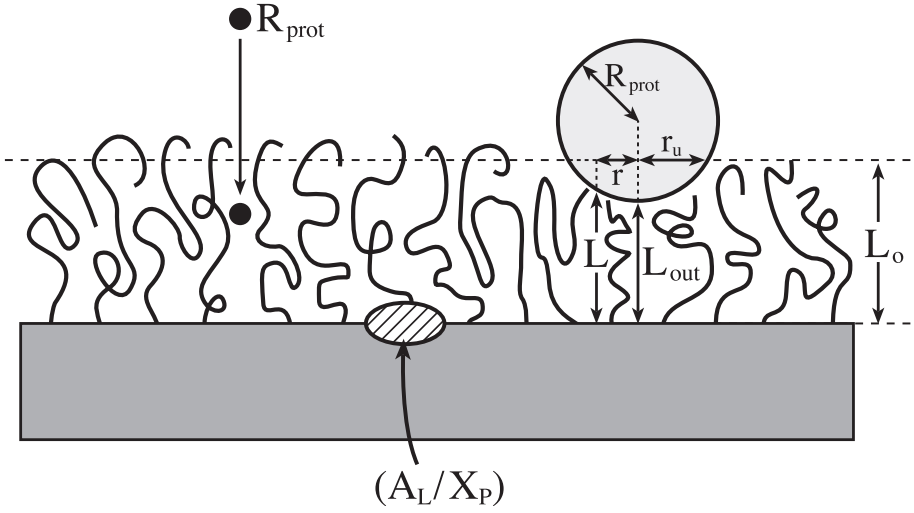

Fig. 15. Left: proteins of small size, R_{prot}, relative to the polymer grafting density, i.e. $\pi R_{prot}^2 < A_l/X_p$, can penetrate the polymer layer and achieve primary adsorption at the lipid surface. Adsorption is diminished, however, by the lateral pressure in the polymer layer. Right: proteins of large size, R_{prot}, relative to the polymer grafting density, i.e. $\pi R_{prot}^2 \gg A_l/X_p$, are unable to penetrate the polymer brush and can achieve only secondary adsorption, possibly at the expense of compressing the brush.

Fig. 15, left). The association constant for primary adsorption, K_{in}, is then given by (see, e.g. Ref. [18]):

$$K_{in}^{ads} = K_{in,o}^{ads}\exp(-\Pi_p A_{prot}/k_B T) \quad (75)$$

where Π_p is the lateral pressure exerted by the polymer layer, A_{prot} ($\approx R_{prot}^2$) is the cross-sectional area of the protein, and $K_{in,o}^{ads}$ is the association constant for the bare lipid surface.

For large proteins, $\pi R_{prot}^2 \gg A_l/X_p$, the protein can adsorb only at the outer surface of the polymer layer (secondary adsorption—see Fig. 15, right). If secondary adsorption is possible, this may be attenuated by compression of the polymer brush. The association constant for secondary adsorption, K_{out}^{ads}, is then given by:

$$K_{out}^{ads} = K_{out,o}^{ads}\exp\{-[F_p(L_{out}) - F_p(L_o)](X_p/A_l)A_{prot}/k_B T\} \quad (76)$$

where $[F_p(L_{out}) - F_p(L_o)](X_p/A_l)$ is the interaction energy per unit area of the polymer brush, L_{out} and L_o are the lengths of the compressed and uncompressed brushes, and $K_{out,o}^{ads}$ is the association constant for secondary adsorption in the absence of polymer lipid. This expression does not allow for any shift in position of the site of secondary adsorption.

7.1. Primary adsorption: small proteins

The lateral pressure, Π_p, exerted in the polymer layer depends on the regime of polymer grafting density. In the low-density mushroom regime, a possible description is the Volmer equation of state [11,47]:

$$\Pi_p^{mush} = \frac{k_B T X_p}{A_l - \pi R_{F3}^2 X_p} \quad (77)$$

where the excluded area per polymer lipid, πR_{F3}^2, is specified by the Flory radius, R_{F3}, given in Eq. (2). This expression is appropriate at low mushroom densities well below the overlap region. Fig. 16 (upper panel) gives predictions based on Eqs. (75) and (77) for the reduction in protein association constant with increasing mole fraction, X_p, of polymer lipid. Dependences on X_p are shown for different polymer and protein sizes that are specified by the composite value $n_p^{6/5}/A_{prot}$ in nm^{-2}. These cover the range of $n_p = 8–114$, corresponding to PEG:350 to PEG:5000, and of $A_{prot} = 6–64$ nm^2 where the higher value corresponds to the cross-sectional area of human serum albumin. The x-axis in the upper panel of Fig. 16 extends up to the mushroom–brush transition of the short PEG:350 polymer (cf. Eq. (4)). The decrease in association constant in Fig. 16 is initially rather modest ($\sim$ 10%). A dramatic decrease is obtained only when the polymer mushrooms approach one another closely and begin to overlap (indicated approximately by the dashed lines in Fig. 16, upper panel). Eq. (77) assumes that proteins do not penetrate the polymer mushrooms appreciably. It

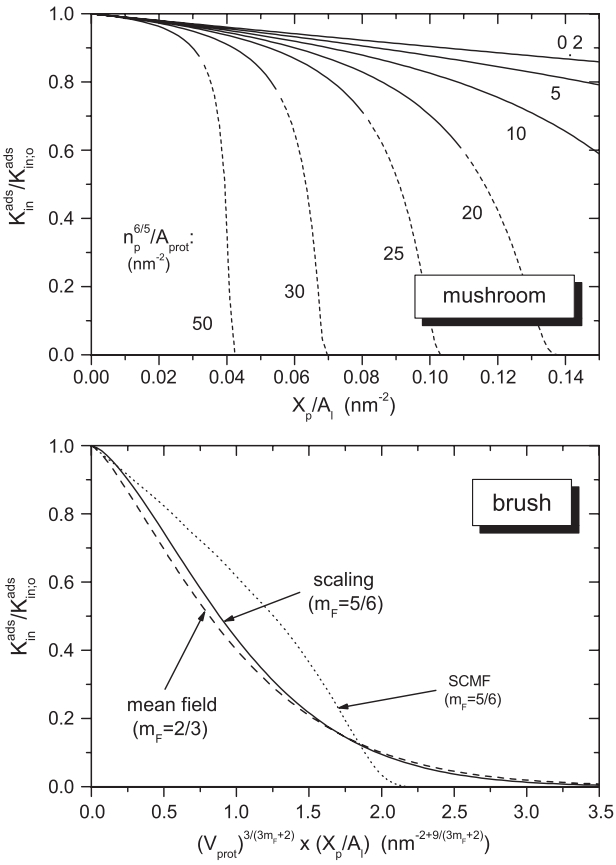

Fig. 16. Dependence of protein primary adsorption, K_{in}^{ads}, on polymer lipid content, X_p, of lipid membranes. Calculations are for $a_m = 0.39$ nm. Upper panel: in the polymer mushroom regime according to Eqs. (75) and (77). Curves are given for different values of polymer length and protein size according to $n_p^{6/5}/A_{prot}$ nm^{-2}, as indicated. These cover the range $A_{prot} = 6–64$ nm^2 and $n_p = 8–114$. Lower panel: in the polymer brush regime according to Eq. (80). The x-axis is normalised with respect to protein volume, V_{prot}, in nm^3. Scaling and mean-field theory results are given by solid and dashed lines, respectively. Dotted line is a numerical SCMF calculation for a small protein, $R_{prot} = 4.86$ a_m [48].

therefore predicts that protein adsorption is abolished at the mushroom–brush transition because then $\Pi_p^{mush} \rightarrow \infty$. This is an overprediction for small proteins that are still able to penetrate the polymer brush.

In the brush regime, the lateral pressure ($\Pi_p^{mush} = -X_p \partial F_p^{brush}/\partial A_l$) exerted by the polymer is given, from Eqs. (7) and (12) by:

$$\Pi_p^{brush} = m_F k_B T n_p a_m^{2m_F} (X_p/A_l)^{m_F+1} \quad (78)$$

where $m_F = 5/6$ for scaling theory and $m_F = 2/3$ in mean-field theory. This pressure is distributed throughout the length, L, of the polymer brush, where L is given by Eq. (6) or Eq. (10). Assuming a uniform stress profile, the lateral pressure experienced by the inserted protein is $(\Pi_p/L) \times 2R_{prot}$, where $2R_{prot}$ is the height of the protein. Eq. (75) therefore becomes:

$$K_{in}^{ads} = K_{in,o}^{ads}\exp[-(\Pi_p^{brush}/L^{brush})V_{prot}/k_B T] \quad (79)$$

where the volume of the protein of molecular weight, M, and partial specific volume, $\bar{v}$, is $V_{\rm prot}=M\bar{v}/N_{\rm A}$, with $N_{\rm A}$ being the Avogadro's number. Substitution from Eqs. (78) and (6) or (10) yields:

$$K_{\rm in}^{\rm ads}=K_{\rm in,o}^{\rm ads}\exp\left[-m_{\rm F}a_{\rm m}^{(2m_{\rm F}-5/3)}V_{\rm prot}(X_{\rm p}/A_{\rm l})^{m_{\rm F}+2/3}\right] \qquad (80)$$

For scaling theory, the exponent of the grafting density, $X_{\rm p}/A_{\rm l}$, is 3/2, and the exponent of $a_{\rm m}$ is zero. This scaling result was obtained by Halperin [46] from the local osmotic pressure by using the "blob" picture of the polymer brush. For mean-field theory, the exponent of $(X_{\rm p}/A_{\rm l})$ is 4/3, and that of $a_{\rm m}$ is $-1/3$. Eq. (80) predicts that adsorption of small proteins is independent of polymer size. This holds for reasonably long polymers, i.e. when the lateral stress profile at the position of the protein is no longer sensitive to polymer length.

Fig. 16 (lower panel) gives predictions of the protein-association constant from Eq. (80) for both scaling theory and mean-field theory, in the brush regime. The x-axis in the lower panel of Fig. 16 is scaled by the protein size, $V_{\rm prot}$, in units of nm^3. Primary protein adsorption declines steeply with increasing content of polymer lipid, after a short initial lag. Adsorption is largely suppressed at grafting densities characterised by an area per polymer, $A_{\rm l}/X_{\rm p}\le R_{\rm prot}^2$, that is of the order of the size of the protein.

A SCMF theory by Szleifer [48] calculates the profile of lateral pressure throughout the polymer brush. This model predicts that the adsorption of a lysozyme model protein ($R_{\rm prot}=4.86a_{\rm m}$) depends on polymer size only for $n_{\rm p}\le 50$. For longer PEG polymers, adsorption is suppressed at a mole fraction of grafting $X_{\rm p}\approx 0.15$. These numerical results are depicted by the dotted line in the lower panel of Fig. 16 for $n_{\rm p}=150$. The dependence on polymer grafting density differs considerably from the predictions of scaling theory or simple mean-field theory for polymer brushes. This is particularly so at low polymer densities for which a brush description becomes less appropriate. Qualitatively, the SCMF data is then more like that predicted for the mushroom regime, in the upper part of Fig. 16.

The kinetics of primary protein adsorption have been treated by Halperin [46]. Kramer's rate theory was used, together with a potential barrier similar to that used in Eq. (50). Additionally, the effective viscosity experienced by the protein in the polymer brush was derived as $\eta\approx\eta_{\rm s}R_{\rm prot}^3(X_{\rm p}/A_{\rm l})^{3/2}$. The largest effect comes, however, from the activation barrier. The reader is referred to the original paper for further details.

7.2. Secondary adsorption: large proteins

Large proteins that are not able to penetrate the polymer brush can only adsorb at the secondary minimum in the potential energy profile [46]. In general, the protein will have to compress the brush to reach the secondary minimum (see Fig. 15, right). This costs energy and the net effect is to resist protein adsorption. Jeon and Andrade [49] analysed this situation for a *flat* protein of area $A_{\rm prot}$, by using Eq. (65) from scaling theory. From Eqs. (65) and (76), the effect of brush compression on the adsorption coefficient is given by:

$$K_{\rm out}^{\rm ads}=K_{\rm out,o}^{\rm ads}\exp\left\{-n_{\rm p}a_{\rm m}^{5/3}A_{\rm prot}\left[\frac{7}{5}\left(\frac{L_{\rm o}^{\rm SC}}{L_{\rm out}}\right)^{5/4}+\left(\frac{L_{\rm out}}{L_{\rm o}^{\rm SC}}\right)^{7/4}-\frac{12}{5}\right]\left(\frac{X_{\rm p}}{A_{\rm l}}\right)^{11/6}\right\} \qquad (81)$$

where $L_{\rm out}$ is the height of the brush at the position of the secondary minimum, and $L_{\rm o}^{\rm SC}$ is given by Eq. (66). Comparable expressions can be derived from MF theory and for the SCMF theory of Milner et al. [12]. From Eq. (59) for MF theory:

$$K_{\rm out}^{\rm ads}=K_{\rm out,o}^{\rm ads}\exp\left\{-n_{\rm p}a_{\rm m}^{4/3}A_{\rm prot}\left[\frac{L_{\rm o}^{\rm MF}}{L_{\rm out}}+\frac{1}{2}\left(\frac{L_{\rm out}}{L_{\rm o}^{\rm MF}}\right)^2-\frac{3}{2}\right]\times\left(\frac{X_{\rm p}}{A_{\rm l}}\right)^{5/3}\right\} \qquad (82)$$

where $L_{\rm o}^{\rm MF}$ is given by Eq. (60). From Eq. (62) for SCMF theory:

$$K_{\rm out}^{\rm ads}=K_{\rm out,o}^{\rm ads}\exp\left\{-\left(\frac{\pi^2}{96}\right)^{1/3}n_{\rm p}a_{\rm m}^{4/3}A_{\rm prot}\times\left[\frac{L^{\rm MWC}}{L_{\rm out}}+\left(\frac{L_{\rm out}}{L^{\rm MWC}}\right)^2-\frac{1}{5}\left(\frac{L_{\rm out}}{L^{\rm MWC}}\right)^5-\frac{9}{5}\right]\left(\frac{X_{\rm p}}{A_{\rm l}}\right)^{5/3}\right\} \qquad (83)$$

where $L^{\rm MWC}$ is given by Eq. (63).

Halperin [46] has treated the situation for secondary adsorption of a spherical protein, by using Eq. (65) from scaling theory, together with the Derjaguin approximation. From simple geometry, the length of the brush at radial distance, r, away from the point of closest contact is given by:

$$L=L_{\rm out}+r^2/2R_{\rm prot} \qquad (84)$$

where $L_{\rm out}$ is the height of the brush at the point of maximum compression and $R_{\rm prot}$ is the radius of the protein (see Fig. 15, right). The Derjaguin approximation for the repulsive potential exerted by the brush on the protein is (cf. Ref. [46]):

$$U_{\rm brush}^{\rm SC}=2\pi\int_0^{r_{\rm u}}[F_{\rm p}^{\rm SC}(L)-F_{\rm p}^{\rm SC}(L_{\rm o}^{\rm SC})](X_{\rm p}/A_{\rm l})r.{\rm d}r \qquad (85)$$

where the integration limits $r=0$ and $r=r_u$ correspond to $L=L_{out}$ and $L=L_o^{SC}$, respectively. Changing variables by means of Eq. (84) leads to:

$$\frac{U_{brush}^{SC}}{K_B T} \approx n_p^2 a_m^{10/3} R_{prot} \left[\frac{7}{5} \left(\frac{L_o^{SC}}{L_{out}} \right)^{1/4} - \frac{1}{11} \left(\frac{L_{out}}{L_o^{SC}} \right)^{11/4} + \frac{3}{5} \left(\frac{L_{out}}{L_o^{SC}} \right) - \frac{21}{11} \right] \left(\frac{X_p}{A_l} \right)^{13/6} \quad (86)$$

where L_o^{SC} is given by Eq. (66). Finally, the modification of the adsorption coefficient from compression of the brush is given by $K_{out}^{ads} = K_{out,o}^{ads} \exp(-U_{brush}/k_B T)$.

The effect of brush compression on the kinetics of protein adsorption has also been considered by Halperin [46]. A semiqualitative approach is used, based on an interaction potential similar to Eq. (86). The reader is referred to the original paper for details.

7.3. Experimental applications

Efremova et al. [38] have studied the adsorption of proteins to supported monolayers of DSPE containing the neutral polymer-grafted lipid SAPDS-PEG:2000. The dependence of the adsorption of bovine pancreatic trypsin inhibitor (BPTI) and human serum albumin (HSA) on polymer grafting density was determined by surface plasma resonance. Results are shown in Fig. 17 in terms of the estimated percentage surface coverage by the adsorbed protein. Adsorption of the larger protein HSA (MW = 66.2 kDa) is suppressed at lower surface grafting densities than is that of the smaller protein BPTI (MW = 6.5 kDa).

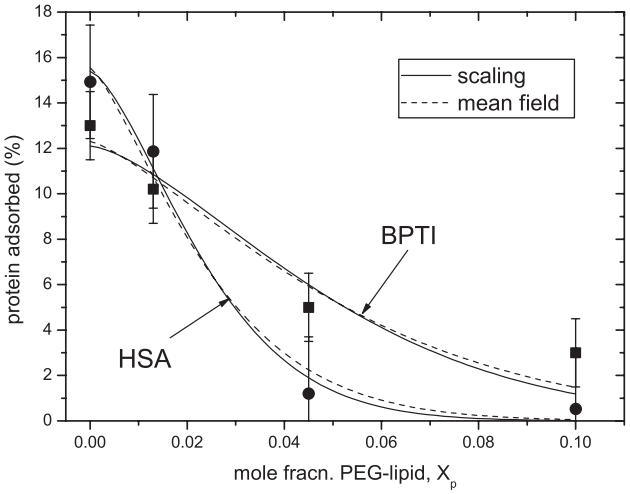

Fig. 17. Adsorption of BPTI and HSA to supported monolayers of DSPE containing PEG:2000-lipid [38]. The solid and dashed lines represent nonlinear least-squares fits of the dependence on polymer grafting density $\sim \exp(-B_m X_p^m)$, where $m = 3/2$ and 4/3 for scaling theory and mean-field theory, respectively (cf. Eq. (80)). For BPTI: $B_{3/2} = 75 \pm 30$ and $B_{4/3} = 45 \pm 15$, and for HSA: $B_{3/2} = 220 \pm 40$ and $B_{4/3} = 120 \pm 30$.

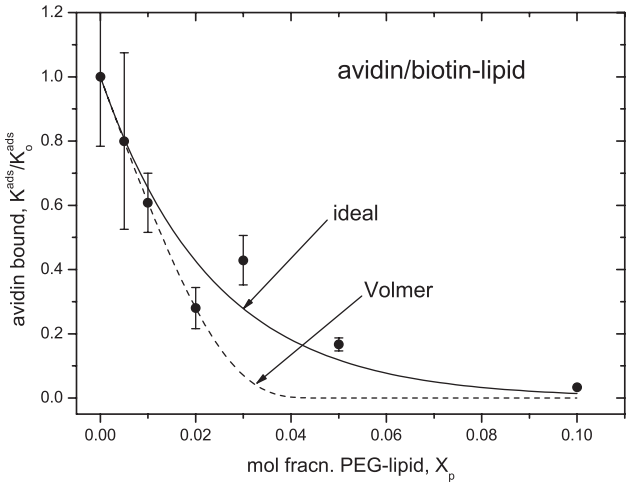

Fig. 18. Binding of avidin to biotinylated giant unilamellar egg phosphatidylcholine vesicles containing DSPE-PEG:750 [50]. Lines represent nonlinear least-squares fits of the dependence on polymer grafting density $\sim \exp[-AX_p/(1-BX_p)]$ (see Eqs. (75) and (77)). Solid line: for ideal-gas lateral pressure ($B=0$) giving $A = 43 \pm 6$ using all data points. Dashed line: for Volmer equation of state, giving $A = 41$, $B = 18$, using just the first four data points.

The solid and dashed lines in Fig. 17 represent least-squares fits of Eq. (80) for scaling theory and mean-field theory, respectively, to the adsorption data. The factor within the exponential that scales the dependence on X_p is used as a fitting parameter, B_m. From Eq. (80) $B_m = (5/6) M\bar{v}/N_A A_l^{3/2}$ for scaling theory and $B_m = (2/3) M\bar{v}/N_A A_l^{4/3}$ for mean-field theory. A value of $A_l = 0.43$ nm^2 was measured for the deposited monolayers. For HSA, this gives predictions of $B_m = 245$ and 170 from scaling and mean-field theories, respectively. These are rather close to the values obtained from the least-squares fits shown in Fig. 17. For BPTI, the predictions are lower than the fitted values: $B_m = 23$ and 22 for scaling and mean-field theories, respectively. It should be remembered, however, that the lower grafting densities shown in Fig. 17 are close to the mushroom regime for a PEG:2000 polymer, whereas Eq. (80) applies to the brush regime.

Studies with spin-labelled lipids (cf. Fig. 6) demonstrate that primary adsorption of HSA to dipalmitoyl phosphatidylcholine membranes is suppressed entirely at the mushroom-to-brush transition, for PEG-lipids with a variety of polymer sizes [11]. For smaller proteins such as BPTI, Fig. 17 shows that protein penetration of the polymer brush is still possible. For PEG:2000-lipids, the mushroom → brush transition is expected to occur at $X_p \sim 0.01$ with gel-phase bilayers (see Eq. (4)). The adsorption of BPTI is not eliminated but is considerably reduced in the brush regime (see Fig. 17).

Noppl-Simson and Needham [50] have measured the binding of avidin to giant phospholipid vesicles that contain biotinylated lipid. Fig. 18 shows the reduction in bound avidin as the polymer-lipid content of the vesicle is increased. Binding is suppressed completely at 10 mol% of PEG-lipid. The decrease in binding depends approximately exponentially on polymer-lipid content (solid line in Fig. 18),

as would be expected for lateral pressure of an ideal gas (cf. Eqs. (75) and (77)). The cross-sectional dimensions of deglycosylated avidin deduced from the crystal structure [51] are $A_{prot}=5.0\times5.6$ nm^2, which yields $A_{prot}/A_l=43$ for $A_l=0.65$ nm^2. This value is close to that obtained from the simple exponential fit in Fig. 18. The effect of using the Volmer equation of state (i.e. Eq. (77)) for the lateral pressure exerted by the polymer mushrooms is shown by the dotted line in Fig. 18. Because Eq. (77) is a hard-disc model, it is predicted that binding is abolished completely at the mushroom–brush transition, i.e. for $X_p\sim0.04-0.05$. For a PEG:750-lipid, Eq. (2) predicts that $\pi R_{F3}^2/A_l\approx22$, which is reasonably close to the value assumed for this model in Fig. 18 (dashed line).

8. Conclusions

The theories of polymer physics go a long way towards establishing design criteria for the polymer-grafted liposomes that are used as carriers in drug delivery. Relatively straightforward approaches allow estimation of the concentrations of polymer lipid that are required to achieve the brush regime that resists adsorption of large proteins. Further considerations outline the contribution to the mechanical properties, the ability to suppress penetration of the polymer brush by small proteins, and the influence on those bilayer properties that affect drug release, particularly of thermosensitive liposomes. An important area is the analysis of the steric repulsive pressure of the polymer, which combats adhesion, particularly to cellular surfaces. Finally, characterisation of the polymer-lipid content at the onset of micelle formation defines the window for which grafted liposomes may be obtained with a stable polymer brush. The possibility that incipient micellisation may improve release properties has still to be investigated.

Definition of symbols used

γ hydrophobic free energy density (i.e. energy per unit area) at the membrane surface
η effective viscosity in the polymer brush
η_s viscosity of the solvent (water)
ϑ degree of surface coverage by adsorbed protein
ν exponent in power-law dependence of the Flory radius on polymer size: $R_{F\hat{d}}\approx a_m n_p^{\nu}$; $\nu=3/(\hat{d}+2)$, where $\hat{d}$ is the dimensionality
ν_e Flory–Huggins excluded volume parameter: $\nu_e=1-2\chi$
ξ_f correlation length of a free polymer in solution
Π_f osmotic pressure of a free polymer in solution
Π_p lateral pressure in the grafted polymer layer
$\Pi_p'(z)$ transverse distribution of lateral pressure in the polymer brush: $\Pi_p'(z)=\partial\Pi_p/\partial z$ where Π_p is the lateral pressure at height z in the polymer brush (units of Π_p' are force per unit area)
Π_p^{brush} lateral pressure of the polymer brush
Π_p^{mush} lateral pressure exerted between polymer mushrooms
Π_{lipid} lateral pressure in the lipid layer
Π_{lipid}^{o} lateral pressure in a bare lipid layer without polymer
ϕ_f volume fraction of a free polymer in solution
$\Phi(z)$ density of polymer chain segments at height z in the brush
χ Flory–Huggins interaction parameter
Ω fractional number of configurations of a confined polymer, relative to a free polymer
a_m effective size, i.e. length, of a monomer unit in a polymer chain
A_l cross-sectional area of a lipid molecule, in the plane of the membrane
$A_{l,o}$ equilibrium area per lipid molecule, in a bare membrane without polymer lipids
ΔA_l expansion in membrane area per lipid molecule by the polymer brush: $\Delta A_l=A_l-A_{l,o}$
ΔA_t change in membrane area, per lipid molecule, at the chain-melting transition
A_{prot} cross-sectional area of a protein
c membrane curvature: $c=1/R^{curv}$, where R^{curv} is the radius of curvature of the membrane
c_o spontaneous mean curvature of the membrane surface: $c_o=1/R_o^{curv}$
c_o^p contribution of the grafted polymer layer to the spontaneous curvature of a single lipid layer
c_1, c_2 principal curvatures of the membrane surface: $c_1=1/R_1^{curv}$, $c_2=1/R_2^{curv}$
C_o strength of repulsive free energy between lipid molecules: $\sim C_o/A_l$
d separation of the surfaces of two adjacent membranes (without the polymer layer)
d_t membrane thickness
$\hat{d}$ dimensionality of space in which the polymer is confined
D distance between polymer grafting points: $D^2=A_l/X_p$
f_o (micelle) fraction of non-polymer lipid, o, that is in a micellar phase
f_p (micelle) fraction of polymer lipid, p, that is in a micellar phase
f_{tot} (micelle) fraction of total lipid that is in a micellar phase
F_{el} elastic free energy for bending of the membrane
F_p free energy of a grafted polymer chain (i.e. free energy per polymer)
F_p^{brush} free energy, per polymer, of the polymer brush
F_p^{MF} free energy of a grafted polymer chain according to mean-field theory (i.e. free energy per polymer)
F_p^{MWC} free energy of a grafted polymer chain according to the SCMF theory of Milner, Witten and Cates (i.e. free energy per polymer)
F_p^{SC} free energy of a grafted polymer chain according to scaling theory (i.e. free energy per polymer)

$F_{\rm int}^{\rm tot}$ total interfacial free energy, per lipid molecule

$F_{\rm R}$ free energy of interaction of a polymer with the confining surface

$\mathcal{F}$ force between crossed cylindrical surfaces in the surface-force apparatus

$\mathcal{F}^{\rm DE}$ force between surfaces in the surface-force apparatus, predicted by Dolan–Edwards theory for the grafted polymer layer

$\mathcal{F}^{\rm MWC}$ force between surfaces in the surface-force apparatus, predicted by the SCMF theory of Milner, Witten and Cates for the grafted polymer layer

$\mathcal{F}^{\rm SC}$ force between surfaces in the surface-force apparatus, predicted by scaling theory for the grafted polymer layer

$k_{\rm B}$ Boltzmann's constant

$k_{\rm c}$ mean curvature bending modulus of a single lipid layer: $k_{\rm c}=\partial M/\partial(c_1+c_2)$ where M is the bending moment acting on a membrane edge, and c_1,c_2 ($=1/R_1^{\rm curv}$, $1/R_2^{\rm curv}$) are the principal curvatures of the membrane (the value for a bilayer membrane is $2\times k_{\rm c}$)

$k_{\rm c}^{\rm lipid}$ contribution from the lipid molecules to the mean curvature modulus

$k_{\rm c}^{\rm o}$ mean curvature modulus of a single bare lipid bilayer without polymer

$k_{\rm c}^{\rm p}$ contribution of the grafted polymer layer to the mean curvature modulus

$\bar{k}_{\rm c}$ Gaussian curvature modulus of a single lipid layer (the value for a bilayer membrane is $2\times\bar{k}c$)

$\bar{k}_{\rm c}^{\rm p}$ contribution of the grafted polymer layer to the Gaussian curvature modulus

$K_{\rm A}$ elastic area-expansion modulus of a single lipid layer: $K_{\rm A}=A_{\rm l}(\partial\tau_{lat}/\partial A_{\rm l})_T$ where $\tau_{\rm lat}$ ($=-\Pi_{\rm lat}$) is the lateral tension in the layer (the value for a bilayer membrane is $2\times K_{\rm A}$)

$K_{\rm A}^{\rm o}$ elastic area-expansion modulus of a single, bare lipid layer, without polymer lipid

$K^{\rm ads}$ equilibrium constant for protein adsorption (Langmuir isotherm)

$K_{\rm in}^{\rm ads}$ association constant for primary adsorption

$K_{\rm in,o}^{\rm ads}$ association constant for primary adsorption to a bare lipid surface

$K_{\rm out}^{\rm ads}$ association constant for secondary adsorption

$K_{\rm out,o}^{\rm ads}$ association constant for secondary adsorption to a bare lipid surface

$L^{\rm MF}$ length of the polymer brush according to mean-field theory: $L^{\rm MF}\approx n_{\rm p}a_{\rm m}^{5/3}(X_{\rm p}/A_{\rm l})^{1/3}$ ($\approx L^{\rm SC}$)

$L_{\rm o}^{\rm MF}$ equilibrium length of a noncompressed polymer brush according to mean-field theory: $L_{\rm o}^{\rm MF}=(k/2)^{1/3}L^{\rm MF}$, where k is an explicit weighting factor introduced into Eq. (5): $F_{\rm p}^{\rm MF}/k_{\rm B}T\approx k(v_{\rm m}n_{\rm p}^2/R)\ (X_{\rm p}/A_{\rm l})+R^2/(n_{\rm p}a_{\rm m}^2)$

$L^{\rm MWC}$ maximum length of the polymer brush according to the SCMF theory of Milner, Witten and Cates

$L_{\rm out}$ thickness of polymer brush when compressed by secondary protein adsorption

$L^{\rm SC}$ length of the polymer brush according to scaling theory: $L^{\rm SC}\approx n_{\rm p}a_{\rm m}^{5/3}(X_{\rm p}/A_{\rm l})^{1/3}$ ($\approx L^{\rm MF}$)

$L_{\rm o}^{\rm SC}$ equilibrium length of a noncompressed polymer brush according to scaling theory: $L_{\rm o}^{\rm SC}=(5k/7)^{1/3}L^{\rm SC}$, where k represents the relative strength of the occluded volume and stretching terms in Eq. (65), which can be expressed alternatively as: $F_{\rm p}^{\rm SC}/k_{\rm B}T\approx L^{\rm SC}(X_{\rm p}/A_{\rm l})^{1/2}[k(L^{\rm SC}/L)^{5/4}+(L/L^{\rm SC})^{7/4}]$

L, $L^{\rm brush}$ thickness of the polymer brush, i.e. height above the membrane surface

$m_{\rm F}$ exponent in dependence of polymer free energy on grafting density: $F_{\rm p}/k_{\rm B}T\approx n_{\rm p}a_{\rm m}^2/(X_{\rm p}/A_{\rm l})m_{\rm F}$; $m_{\rm F}=5/6$ for scaling theory and $m_{\rm F}=2/3$ for mean-field theory

$m_{\rm F}'$ exponent in the scaling theory for the free energy of a compressed polymer mushroom

$m_{\rm L}$ exponent in scaling theory for polymer length

$m_{\rm R}'$ exponent in the scaling theory for the radus of a compressed polymer mushroom

$n_{\rm p}$ number of monomers per polymer (p), i.e. polymer length/degree of polymerisation

$N_{\rm A}$ Avogadro's number

P applied osmotic pressure

$P_{\rm R}$ repulsive pressure between membranes

$P^{\rm MF}$ pressure required to compress a polymer mushroom (from mean-field theory)

$P_{\rm R}^{\rm MF}$ repulsive pressure between membranes according to mean-field theory for the grafted polymer layer

$P_{\rm R}^{\rm MWC}$ repulsive pressure between membranes according to the SCMF theory of Milner, Witten and Cates for the grafted polymer layer

$P_{\rm R}^{\rm osm}$ osmotic contribution to the repulsive pressure between membranes, for overlapping grafted polymer chains

$P_{\rm R}^{\rm SC}$ repulsive pressure between membranes according to scaling theory for the grafted polymer layer

R end-to-end distance of a polymer chain

$R^{\rm curv}$ local radius of curvature of the membrane

$R_{\rm o}^{\rm curv}$ spontaneous radius of curvature of the membrane surface

$R_1^{\rm curv}$, $R_2^{\rm curv}$ principal radii of curvature of the membrane surface

$R_{\rm F}$ Flory radius of a random-coil polymer chain

$R_{\rm F2}$ Flory radius of a random coil polymer that is confined to two dimensions: $R_{\rm F2}\approx a_{\rm m}n_{\rm p}^{3/4}$

$R_{\rm F3}$ Flory radius of a random-coil polymer in three dimensions: $R_{\rm F3}\approx a_{\rm m}n_{\rm p}^{3/5}$

$R_{\rm F3}^{\rm o}$ Flory radius of a noncompressed polymer mushroom: $R_{\rm F3}^{\rm o}=(3k/2)^{1/5}R_{\rm F3}$, where k is an explicit weighting factor introduced into Eq. (1): $F_{\rm p}/k_{\rm B}T=k(v_{\rm m}n_{\rm p}^2/R^3)+R^2/(n_{\rm p}a_{\rm m}^2)$

$R_{{\rm F}\hat{d}}$ Flory radius of a random-coil polymer in $\hat{d}$ dimensions

$R_{\rm prot}$ protein radius

$\Delta S_{\rm t}$ transition entropy for chain melting of a lipid membrane

T	absolute temperature
T_t	chain-melting transition temperature of a lipid membrane
ΔT_t	shift in chain-melting transition temperature of a lipid membrane
v_m	excluded volume per monomer of the polymer chain
V_{prot}	volume of a protein molecule
$\bar{v}$	partial specific volume
X_p	mole fraction of polymer lipid, p
X_p^{end}	mole fraction of polymer lipid at the completion of micelle formation
X_p^{on}	mole fraction of polymer lipid at the onset of micelle formation
$X_p^{m \rightarrow b}$	mole fraction of polymer lipid at which the polymer layer converts from the mushroom regime to the brush regime
z	vertical height in the membrane (in the direction of the normal to the membrane surface)

Acknowledgements

Work of the authors on PEG-lipids is supported by a research grant in the framework of the CIPE project CLUSTER MIA26-P5B. The authors are members of the European COST-D22 Action.

References

[1] P.J. Flory, Principles of Polymer Chemistry, Cornell Univ. Press, Ithaca, NY, 1971.
[2] P.G. De Gennes, Scaling Concepts in Polymer Physics, Cornell Univ. Press, London, 1979.
[3] S. Alexander, Adsorption of chain molecules with a polar head. A scaling description, J. de Phys. 38 (1977) 983–987.
[4] P.G. De Gennes, Conformations of polymers attached to an interface, Macromolecules 13 (1980) 1069–1075.
[5] K. Hristova, D. Needham, Phase behavior of a lipid/polymer–lipid mixture in aqueous medium, Macromolecules 28 (1995) 991–1002.
[6] E. Evans, D.J. Klingenberg, W. Rawicz, F. Szoka, Interactions between polymer-grafted membranes in concentrated solutions of free polymer, Langmuir 12 (1996) 3031–3037.
[7] A.K. Kenworthy, K. Hristova, D. Needham, T.J. McIntosh, Range and magnitude of the steric pressure between bilayers containing phospholipids with covalently attached poly(ethylene glycol), Biophys. J. 68 (1995) 1921–1936.
[8] K. Hristova, A. Kenworthy, T.J. McIntosh, Effect of bilayer composition on the phase behaviour of liposomal suspensions containing poly(ethylene glycol)-lipids, Macromolecules 28 (1995) 7693–7699.
[9] D. Marsh, Handbook of Lipid Bilayers, CRC Press, Boca Raton, FL, 1990.
[10] G. Montesano, R. Bartucci, S. Belsito, D. Marsh, L. Sportelli, Lipid membrane expansion and micelle formation by polymer-grafted lipids: scaling with polymer length studied by spin-label electron spin resonance, Biophys. J. 80 (2001) 1372–1383.
[11] R. Bartucci, M. Pantusa, D. Marsh, L. Sportelli, Interaction of human serum albumin with membranes containing polymer-grafted lipids: spin-label ESR studies in the mushroom and brush regimes, Biochim. Biophys. Acta 1564 (2002) 237–242.
[12] S.T. Milner, T.A. Witten, M.E. Cates, A parabolic density profile for grafted polymers, Europhys. Lett. 5 (1988) 413–418.
[13] S.T. Milner, T.A. Witten, M.E. Cates, Theory of the grafted polymer brush, Macromolecules 21 (1988) 2610–2619.
[14] P. Pincus, Colloid stabilization with grafted polyelectrolytes, Macromolecules 24 (1991) 2912–2919.
[15] M. Daoud, P.G. De Gennes, Statistics of macromolecular solutions trapped in small pores, J. de Phys. 38 (1977) 85–93.
[16] P.L. Hansen, J.A. Cohen, R. Podgornik, V.A. Parsegian, Osmotic properties of poly(ethylene glycols): quantitative features of brush and bulk scaling laws, Biophys. J. 84 (2003) 350–355.
[17] T.L. Kuhl, D.E. Leckband, D.D. Lasic, J.N. Israelachvili, Modulation of interaction forces between bilayers exposing short-chained ethylene oxide headgroups, Biophys. J. 66 (1994) 1479–1488.
[18] D. Marsh, Lateral pressure in membranes, Biochim. Biophys. Acta 1286 (1996) 183–223.
[19] D. Marsh, Elastic constants of polymer-grafted lipid membranes, Biophys. J. 81 (2001) 2154–2162.
[20] J.N. Israelachvili, S. Marcelja, R.G. Horn, Physical principles of membrane organization, Q. Rev. Biophys. 13 (1980) 121–200.
[21] G. Cevc, D. Marsh, Phospholipid Bilayers. Physical Principles and Models, Wiley-Interscience, New York, 1987.
[22] D.D. Lasic, D. Needham, The "stealth" liposome: a prototypical biomaterial, Chem. Rev. 95 (1995) 2601–2628.
[23] K. Hristova, D. Needham, The influence of polymer-grafted lipids on the physical properties of lipid bilayers: a theoretical study, J. Colloid Interface Sci. 168 (1994) 302–314.
[24] M. Pantusa, R. Bartucci, D. Marsh, L. Sportelli, Shifts in chain-melting transition temperature of liposomal membranes by polymer-grafted lipids, Biochim. Biophys. Acta 1614 (2003) 165–170.
[25] K. Hashizaki, C. Itoh, H. Sakai, S. Yokohama, H. Taguchi, Y. Saito, N. Ogawa, M. Abe, Freeze-fracture electron microscopic and calorimetric studies on microscopic states of surface-modified liposomes with poly(ethylene glycol) chains, Colloids Surf., B 17 (2000) 275–282.
[26] G.R. Anyarambhatla, D. Needham, Enhancement of the phase transition permeability of DPPC liposomes by incorporation of MPPC: a new temperature-sensitive liposome for use with mild hyperthermia, J. Liposome Res. 9 (1999) 491–506.
[27] D. Needham, G. Anyarambhatla, G. Kong, M.W. Dewhirst, A new temperature-sensitive liposome for use with mild hyperthermia: characterization and testing in a human tumor xenograft model, Cancer Res. 60 (2000) 1197–1201.
[28] E.A. Evans, R. Skalak, Mechanics and Thermodynamics of Biomembranes, CRC Press, Boca Raton, FL, 1980.
[29] D. Needham, T.J. McIntosh, D.D. Lasic, Repulsive interactions and mechanical stability of polymer-grafted lipid membranes, Biochim. Biophys. Acta 1108 (1992) 40–48.
[30] S.T. Milner, T.A. Witten, Bending moduli of polymeric surfactant interfaces, J. Phys. 49 (1988) 1951–1962.
[31] M. Bloom, E. Evans, O.G. Mouritsen, Physical properties of the fluid lipid-bilayer component of cell membranes: a perspective, Q. Rev. Biophys. 24 (1991) 293–397.
[32] I. Szleifer, D. Kramer, A. Benshaul, W.M. Gelbart, S.A. Safran, Molecular theory of curvature elasticity in surfactant films, J. Chem. Phys. 92 (1990) 6800–6817.
[33] D. Marsh, Intrinsic curvature in normal and inverted lipid structures and in membranes, Biophys. J. 70 (1996) 2248–2255.
[34] T.R. Baekmark, S. Pedersen, K. Jørgensen, O.G. Mouritsen, The effects of ethylene oxide containing lipopolymers and tri-block copolymers on lipid bilayers of dipalmitoylphosphatidylcholine, Biophys. J. 73 (1997) 1479–1491.
[35] S. Rex, M.J. Zuckermann, M. Lafleur, J.R. Silvius, Experimental and Monte Carlo simulation studies of the thermodynamics of polyethyleneglycol chains grafted to lipid bilayers, Biophys. J. 75 (1998) 2900–2914.
[36] S. Belsito, R. Bartucci, G. Montesano, D. Marsh, L. Sportelli, Mo-

lecular and mesoscopic properties of hydrophilic polymer-grafted phospholipids mixed with phosphatidylcholine in aqueous dispersion: interaction of dipalmitoyl *N*-poly(ethylene glycol)phosphatidylethanolamine studied by spectrophotometry and spin-label electron spin resonance, Biophys. J. 78 (2000) 1420–1430.
[37] J.N. Israelachvili, Intermolecular and Surface Forces, Academic Press, London, 1985.
[38] N.V. Efremova, B. Bondurant, D.F. O'Brien, D.E. Leckband, Measurements of interbilayer forces and protein adsorption on uncharged lipid bilayers displaying poly(ethylene glycol) chains, Biochemistry 39 (2000) 3441–3451.
[39] A.K. Dolan, S.F. Edwards, Theory of stabilization of colloids by adsorbed polymer, Proc. R. Soc. Lond., A 337 (1974) 509–516.
[40] S. Patel, M. Tirrell, G. Hadziioannou, A simple model for forces between surfaces bearing grafted polymers applied to data on adsorbed block copolymers, Colloids Surf. 31 (1988) 157–179.
[41] B.V. Derjaguin, Untersuchungen über die Reibung und Adhäsion: IV. Theorie des Anhaftens kleiner Teilchen, Kolloid-Z. 69 (1934) 155–164.
[42] J. Marra, J. Israelachvili, Direct measurements of forces between phosphatidylcholine and phosphatidylethanolamine bilayers in aqueous electrolyte solutions, Biochemistry 24 (1985) 4608–4618.
[43] E. Evans, D. Needham, Attraction between lipid bilayer membranes in concentrated solutions of nonadsorbing polymers: comparison of mean-field theory with measurements of adhesion energy, Macromolecules 21 (1988) 1822–1831.
[44] J.F. Joanny, L. Leibler, P.G. De Gennes, Effects of polymer solutions on colloid stability, J. Polym. Sci., B, Polym. Phys. 17 (1979) 1073–1084.
[45] T. Heimburg, D. Marsh, Thermodynamics of the interaction of proteins with lipid membranes, in: K.M. Merz Jr., B. Roux (Eds.), Biological Membranes, Birkhäuser, Boston, 1996, pp. 405–462.
[46] A. Halperin, Polymer brushes that resist adsorption of model proteins: design parameters, Langmuir 15 (1999) 2525–2533.
[47] D. Needham, N. Stoicheva, D.V. Zhelev, Exchange of monooleoylphosphatidylcholine as monomer and micelle with membranes containing poly(ethylene glycol)-lipid, Biophys. J. 73 (1997) 2615–2629.
[48] I. Szleifer, Protein adsorption on surfaces with grafted polymers: a theoretical approach, Biophys. J. 72 (1997) 595–612.
[49] S.I. Jeon, J.D. Andrade, Protein surface interactions in the presence of polyethylene oxide: 2. Effect of protein size, J. Colloid Interface Sci. 142 (1991) 159–166.
[50] D.A. Noppl-Simson, D. Needham, Avidin–biotin interactions at vesicle surfaces: adsorption and binding, cross-bridge formation, and lateral interactions, Biophys. J. 70 (1996) 1391–1401.
[51] L. Pugliese, A. Coda, M. Malcovati, M. Bolognesi, Three-dimensional structure of the tetragonal crystal form of egg-white avidin in its functional complex with biotin at 2.7 Å resolution, J. Mol. Biol. 231 (1993) 698–710.